LETTER

High–avidity IgA protects the intestine by enchaining growing bacteria

Kathrin Moor[1]†, Médéric Diard[1], Mikael E. Sellin[1,2], Boas Felmy[1], Sandra Y. Wotzka[1], Albulena Toska[1], Erik Bakkeren[1], Markus Arnoldini[1], Florence Bansept[3], Alma Dal Co[4,5], Tom Völler[1], Andrea Minola[6], Blanca Fernandez-Rodriguez[7], Gloria Agatic[6], Sonia Barbieri[7], Luca Piccoli[7], Costanza Casiraghi[7]†, Davide Corti[6], Antonio Lanzavecchia[1,7], Roland R. Regoes[8], Claude Loverdo[3], Roman Stocker[9], Douglas R. Brumley[9,10]*, Wolf-Dietrich Hardt[1]* & Emma Slack[1]*

Vaccine-induced high-avidity IgA can protect against bacterial enteropathogens by directly neutralizing virulence factors or by poorly defined mechanisms that physically impede bacterial interactions with the gut tissues ('immune exclusion')[1–3]. IgA-mediated cross-linking clumps bacteria in the gut lumen and is critical for protection against infection by non-typhoidal *Salmonella enterica* subspecies enterica serovar Typhimurium (*S.* Typhimurium). However, classical agglutination, which was thought to drive this process, is efficient only at high pathogen densities ($\geq 10^8$ non-motile bacteria per gram). In typical infections, much lower densities[4,5] (10^0–10^7 colony-forming units per gram) of rapidly dividing bacteria are present in the gut lumen. Here we show that a different physical process drives formation of clumps *in vivo*: IgA-mediated cross-linking enchains daughter cells, preventing their separation after division, and clumping is therefore dependent on growth. Enchained growth is effective at all realistic pathogen densities, and accelerates pathogen clearance from the gut lumen. Furthermore, IgA enchains plasmid-donor and -recipient clones into separate clumps, impeding conjugative plasmid transfer *in vivo*. Enchained growth is therefore a mechanism by which IgA can disarm and clear potentially invasive species from the intestinal lumen without requiring high pathogen densities, inflammation or bacterial killing. Furthermore, our results reveal an untapped potential for oral vaccines in combating the spread of antimicrobial resistance.

Antibody-mediated agglutination is used for strain-typing[6,7], a method in which surface-epitope-binding antibodies are mixed with high-density bacterial suspensions. When bacteria collide, they are cross-linked by the antibody and form clumps. Agglutination is thought to operate *in vivo* to promote IgA-mediated immune exclusion[1,2,8,9]. Indeed, IgA can clump *Salmonella* spp., *Vibrio cholerae* and *Enterococcus faecalis* in the gut[8–10]. However, as collision rates (and therefore agglutination) increase with the square of the bacterial density[11], agglutination is expected to be inefficient at lower densities (below typical[4,12] densities of 10^8 colony-forming units (CFU) g^{-1} in our model; see Supplementary Information). Alternative mechanisms of IgA-mediated protection (for example, flagella blockage and bacterial cell disruption) have been reported[13–17], but it remains unclear how IgA protects *in vivo*[2] (Fig. 1a).

We studied high-avidity IgA-mediated protection using the streptomycin mouse model of non-typhoidal salmonellosis[18]. Inoculum sizes from 10^1 to 10^{10} CFU yield reproducible infections and the initial pathogen growth rate in the gut lumen is independent of the

inoculum size (doubling time $= 30 \pm 5$ min) until the maximum gut luminal pathogen density of 10^9 CFU g^{-1} is achieved, and growth then markedly slows[19] (Extended Data Fig. 1). *S.* Typhimurium invasion into the gut tissue promotes typhlocolitis and systemic spread[18,20]. These processes are not affected by low-avidity 'natural IgA'[18,20]. However, we can induce high-avidity, disease-protective, lipopolysaccharide-binding IgA by oral vaccination with a peracetic-acid-inactivated *S.* Typhimurium SL1344 strain (PA-*S*.Tm)[21]. This allowed us to investigate the functions of high-avidity IgA at a wide range of pathogen densities.

To explore IgA function with realistic inocula[4], mice that were vaccinated with PA-*S*.Tm or mock-vaccinated (with phosphate-buffered solution (PBS) only) were infected with 10^5 CFU wild-type *S.* Typhimurium (Supplementary Tables 1 and 2) by gavage. Vaccine-elicited IgA prevented colonization of the mesenteric lymph nodes (mLN), invasion of caecal tissue and induction of intestinal inflammation by wild-type *S.* Typhimurium[8,21] (Fig. 1b–d, Extended Data Fig. 2a, b). In vaccinated mice, gut luminal *S.* Typhimurium were coated and efficiently clumped by IgA in a lipopolysaccharide O-antigen-dependent manner (Fig. 1e–g, Extended Data Fig. 2c). Many clumps contained more than 50 bacteria after 18 h (Fig. 1f, g, Extended Data Fig. 2d, e).
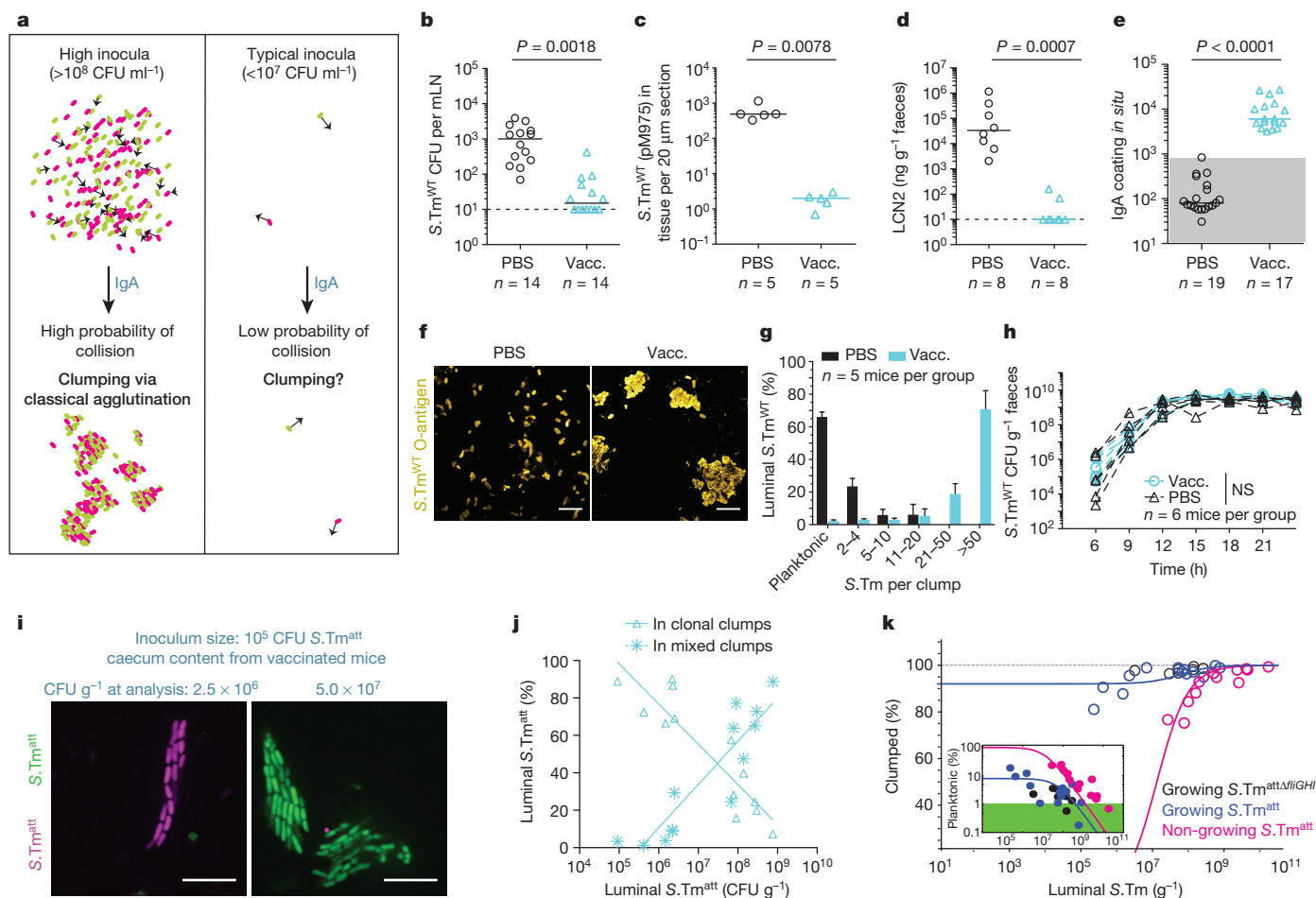
On close examination, previous hypotheses of IgA function[13,14,16,17] were not sufficient to explain the observed protection. Classical agglutination is inefficient at lower pathogen densities (Supplementary Information), such as those typically observed in human and animal *S.* Typhimurium infections[4,5]. Gut luminal growth analysis excluded direct toxicity (Fig. 1h, Extended Data Fig. 3). We could also exclude a major role for virulence factor neutralization. Although IgA can impair flagella-driven motility and this is expected to attenuate *S.* Typhimurium (Extended Data Fig. 4a–c), vaccination efficiently protected against *S.* Typhimurium strains that were deficient for flagella and/or type III secretion systems 1 and 2 (Extended Data Fig. 4d–f). Instead, IgA sequestered *S.* Typhimurium deep inside the gut luminal space (Extended Data Fig. 4g, h). Thus, clumping took place before pathogens could interact with the gut epithelium through type III secretion systems 1 and 2.

To test whether clumping alone was sufficient to protect, we analysed infections with barcoded wild-type *S.* Typhimurium through a stochastic immigration–growth–clearance model for mLN colonization[22] (Extended Data Fig. 5). Clumping-mediated reductions in planktonic, infectious wild-type *S.* Typhimurium cells could fully account for the reduced mLN colonization observed

[1]Institute of Microbiology, ETH Zürich, 8093 Zürich, Switzerland. [2]Science for Life Laboratory, Department of Medical Biochemistry and Microbiology, Uppsala University, 75124 Uppsala, Sweden. [3]Laboratoire Jean Perrin (UMR 8237), CNRS - UPMC, 75005 Paris, France. [4]Department of Environmental Systems Science, ETH Zurich, Zürich, Switzerland. [5]Department of Environmental Microbiology, Eawag, Swiss Federal Institute of Aquatic Science and Technology, Dübendorf, Switzerland. [6]Humabs BioMed SA, 6500 Bellinzona, Switzerland. [7]Institute for Research in Biomedicine, Università della Svizzera italiana, Bellinzona 6500, Switzerland. [8]Institute of Integrative Biology, ETH Zürich, 8092 Zürich, Switzerland. [9]Institute of Environmental Engineering, Department of Civil, Environmental, and Geomatic Engineering, ETH Zürich, 8093 Zürich, Switzerland. [10]School of Mathematics and Statistics, The University of Melbourne, Parkville, Victoria 3010, Australia. †Present addresses: Center for Dental Medicine, University of Zürich, Zürich, Switzerland (K.M.); Department of Experimental, Diagnostic and Specialty Medicine, University of Bologna, Bologna, Italy (C.C.).
*These authors contributed equally to this work.

Figure 1 | Enchained growth is a protective mechanism in non-typhoidal salmonellosis. a, Density-dependence of agglutination. **b–g**, Mock- (PBS) or PA-S.Tm-vaccinated (vacc.) mice were pretreated with streptomycin, infected (10^5 CFU, indicated strain, by gavage) and analysed 18 h later. Pathogen loads in mLN (CFU) (**b**) or epithelium and lamina propria (microscopy[20]) (**c**). **d**, Faecal lipocalin-2 (LCN2). **e**, IgA-coating of wild-type S. Typhimurium (S.Tm^WT) (caecum content; see Extended Data Fig. 2). **f**, **g**, S. Typhimurium clumping in caecum lumen (frozen sections; scale bar, 10 μm; mean ± s.d.). **h**, Faecal S.Tm^WT (see Extended Data Fig. 3). NS, not significant (repeat-measures ANOVA). **i–k**, PA-S.Tm-vaccinated mice were challenged with a 1:1-mix of mCherry- and GPF-tagged S.Tm^att (10^5 CFU). Images of live caecal

content (3–8 h after infection). **i**, Representative images (5 h after infection). **j**, Clump clonality (representative images in Extended Data Fig. 6d) plotted against luminal CFU density ($n = 13$). **k**, Confocal microscopy quantification of clumping from mice infected with 10^5 CFU S.Tm^att (blue circles, $n = 13$) or S.Tm^{att Δ fliGHI} (black circles, $n = 7$) and 10^{10} CFU S.Tm^att or 10^9 PFA-fixed S.Tm^att (magenta circles, $n = 12$). Lines show robust fittings of the enchained growth/agglutination model, green area represents parameter space where less than 1% luminal S.Tm are planktonic (see Supplementary Information; Extended Data Fig. 7). Dashed line, detection limit; grey-shaded areas, background levels. Unless otherwise stated, statistics are the results of two-tailed Mann–Whitney U-tests. Horizontal lines represent median.
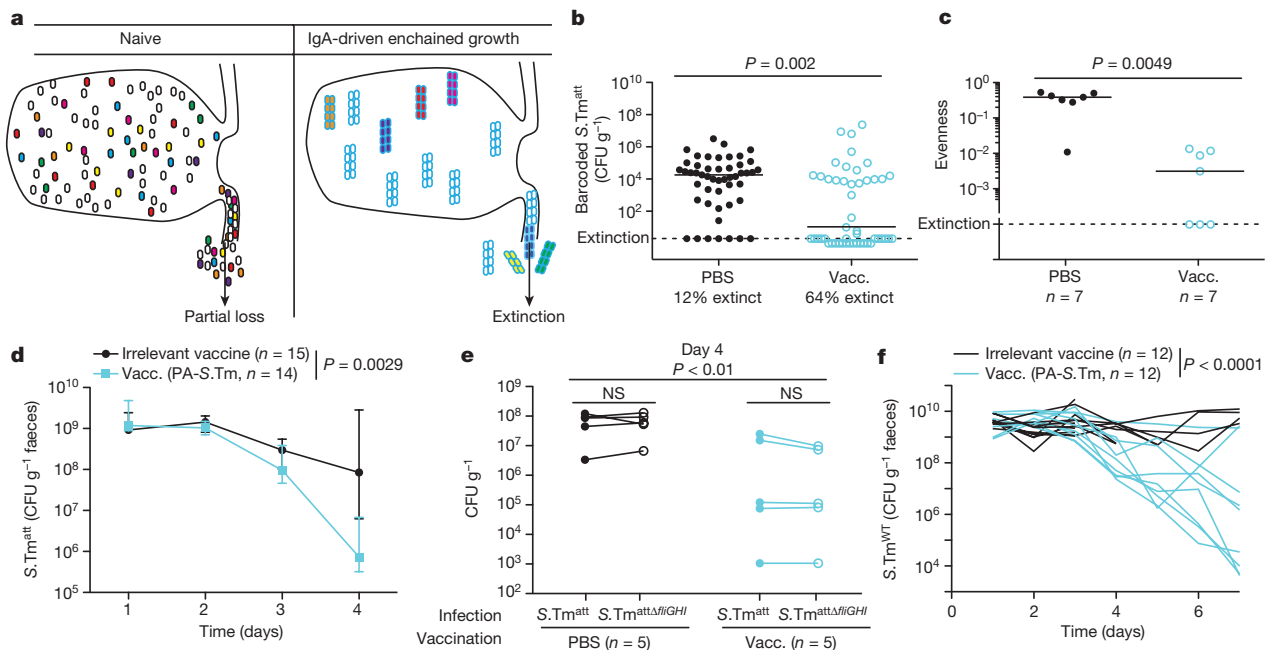
(Extended Data Fig. 5b–e). As agglutination cannot drive clumping at lower pathogen densities, these observations suggested a gap in our understanding of immune exclusion.

We hypothesized that IgA-mediated enchainment of daughter cells immediately after division would be an alternative, density-independent mechanism of clump formation: a process termed 'enchained growth'. To investigate this, we infected PA-S.Tm-vaccinated mice with a 1:1 mixture of GFP-tagged and mCherry-tagged attenuated S. Typhimurium (S.Tm^att) (10^5 CFU by gavage; attenuated mutant used to avoid inflammation in mock-vaccinated controls). Live microscopy revealed that most S.Tm^att were present in uniformly GFP^+ or mCherry^+ clumps, particularly when pathogen densities were below 10^8 CFU g^{-1} (Fig. 1i, j). This clonal structure supports clumping by IgA-driven enchained growth. Importantly, enchained growth is driven by bacterial growth, rather than bacterial collisions (which would depend on cell density and movement) and is therefore dependent on physical processes that are different to those that drive classical agglutination (Supplementary Information).

Although enchained growth dominated IgA-driven clumping at low to moderate population densities, we could observe well-mixed clumps

(indicative of classical agglutination) early after infection with 10^{10} CFU (Extended Data Fig. 6a, b). As soon as S. Typhimurium began to grow, classical agglutination was complemented by enchained growth (Extended Data Fig. 6c). Correspondingly, at high S. Typhimurium densities, clonal clumps coalesced into large oligoclonal clumps (Fig. 1j, k, Extended Data Fig. 6d–f). Thus, enchained growth occurs in all situations in which IgA-coated bacteria grow in the gut lumen, whereas classical agglutination is only observed at high S. Typhimurium densities.

To determine how enchained growth and classical agglutination contribute to clumping (that is, immune exclusion), we devised a mathematical model describing the gut luminal planktonic S. Typhimurium density (Extended Data Fig. 7, Supplementary Information). We assumed that both classical agglutination and enchained growth depended on IgA cross-linking efficiency, but that enchained growth depended on the bacterial growth rate, whereas classical agglutination depended on the bacterial collision rate. The model quantitatively predicted experimental data describing the extent to which IgA-mediated clumping of growing and non-growing S. Typhimurium occurred in the caecal lumen of vaccinated mice

Figure 2 | Enchained growth drives clonal extinction and clearance from the caecal lumen. a, *S.* Typhimurium growth in the caecum of naive or vaccinated mice. Fill-colours represent barcodes. Blue lines represent the secretory IgA-coat. **b**, Mock- or PA-*S.*Tm-vaccinated mice (vacc.) were challenged with $S.\text{Tm}^{att}$ (10^5 CFU total) spiked with approximately 10 CFU of each of seven genetically barcoded $S.\text{Tm}^{att}$ strains. Barcoded $S.\text{Tm}^{att}$ was quantified in the caecal lumen after 18 h. The percentage of barcoded strains that become undetectable ('extinct') is shown. **c**, 'Evenness'[26] of

clone representation for each mouse. **d, e**, Mock- or PA-*S.*Tm-vaccinated mice were orally infected with 10^5 CFU of $S.\text{Tm}^{att}$ alone, or a 1:1 mixture of $S.\text{Tm}^{att}$ and $S.\text{Tm}^{att\Delta fliGHI}$. Faecal CFU were determined at days 1–4 (**d**, median and interquartile range) or day 4 (**e**). **f**, 129S6/SvEvTac mice ($n = 12$ per group at the start) were vaccinated with PA-*S.*Tm or an irrelevant vaccine and infected (10^5 CFU $S.\text{Tm}^{WT}$). Faecal shedding was analysed. Repeat-measures ANOVA on log-normalized data, pooled from two independent experiments.

(Fig. 1k, Extended Data Fig. 7a–c; Supplementary Information). Both model and *in vivo* data predicted that classical agglutination is inefficient at *S.* Typhimurium densities below 10^8 CFU g^{-1} (Fig. 1k), the maximum density typically observed in human non-typhoidal salmonellosis[12]. At less than 10^8 CFU g^{-1}, the probability of collision was too low, even when IgA cross-linking strength was high, and enchained growth therefore dominated clump formation (Fig. 1k, Supplementary Information). Extrapolation predicts that enchained growth would reduce the density of planktonic, invasive *S.* Typhimurium cells by 90%, even at densities below 10^2 CFU g^{-1} (Fig. 1k, Supplementary Information). IgA-driven enchained growth is therefore a fundamentally distinct process from classical agglutination. Enchained growth restrains the targeted bacteria in a density-independent, growth-dependent manner, and dominates clumping in natural *S.* Typhimurium infections of immunized hosts.
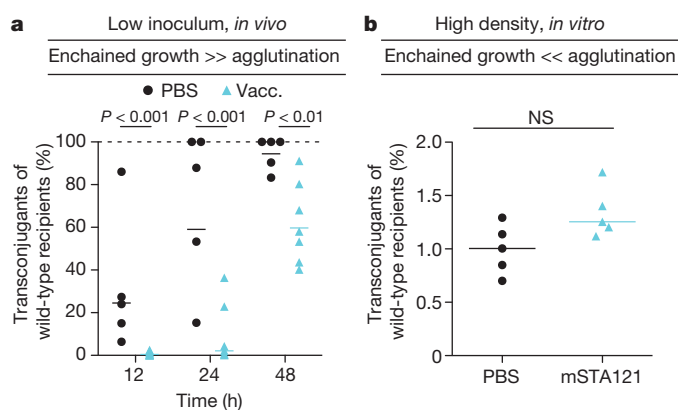
IgA-driven enchained growth also affects the evolvability of *S.* Typhimurium in the gut lumen. Bacteria exist as metapopulations of clones that acquire mutations[23] and exchange DNA[24]. Enchained growth confines these clones into separate clumps (Fig. 1i, j, Extended Data Fig. 6) that have a limited ability to interact with each other while travelling in the faecal stream. This reduces the effective evolutionary population size in a way that, to our knowledge, is not described by common models in population genetics. Three testable hypotheses can be derived from this: the *en bloc* loss of whole enchained clones should (1) increase clonal extinction rates and (2) accelerate pathogen clearance from the gut, and (3) enchained growth should inhibit contact-dependent horizontal gene transfer, by separating donor and recipient clones.

First, increased clonal extinction occurs because IgA-enchained monoclonal clumps are lost from the caecum as single entities (Fig. 2a). This was analysed *in vivo* by spiking 10–100 CFU of barcoded *S.* Typhimurium clones[22,25,26] into the inoculum (10^5 CFU total) and quantifying luminal barcode retention after 18 h. Clonal

extinction was more pronounced in PA-*S.*Tm-vaccinated mice than in mock-vaccinated mice (Fig. 2b, c), as predicted by mathematical modelling (Extended Data Fig. 8). This was not attributable to direct toxicity of IgA. A monoclonal dimeric IgA directed against the O-12 epitope of *S.* Typhimurium O-antigen (data not shown) or purified intestinal IgA (Extended Data Fig. 9a–d) did not affect *S.* Typhimurium growth *in vitro*. Further, under high inoculum conditions (10^{10} CFU *S.* Typhimurium, dominant classical agglutination), the clonal extinction rate was indistinguishable between PA-*S.*Tm- and mock-vaccinated mice (Extended Data Fig. 9e–g). Therefore, enchained growth can accelerate clonal extinction from the gut lumen.

Second, the *en bloc* loss of clumped *S.* Typhimurium should accelerate microbiota-driven clearance[8] from the gut lumen of vaccinated mice. In mice that are pretreated with streptomycin and then infected with $S.\text{Tm}^{att}$, this starts between day 3 and 4 after infection[8]. Accordingly, high-avidity IgA accelerated clearance of $S.\text{Tm}^{att}$ from the intestinal lumen (Fig. 2d). Loss of flagella-driven motility does not contribute to this effect, as a co-infection of $S.\text{Tm}^{att}$ and $S.\text{Tm}^{att\Delta fliGHI}$ (mutant strain also lacking flagella) led to equal clearance of both strains in vaccinated and unvaccinated mice (Fig. 2e). As inflammation suppresses microbiota regrowth after antibiotic-treatment[27], vaccine-induced IgA has a dual role in promoting *S.* Typhimurium luminal clearance during wild-type *S.* Typhimurium infection (Fig. 2f). Enchained growth both clumps and aids clearance of growing *S.* Typhimurium. Further, blockade of intestinal inflammation (Fig. 1d) avoids collateral damage to the microbiota[8], thereby enhancing competitive pathogen elimination from the gut lumen.

Third, the separation into clonal clumps should prohibit plasmid transfer, as conjugation requires direct physical contact between donor and recipient clones. This was analysed by co-infecting mice with a recipient (plasmid-lacking) strain and a donor strain containing a chloramphenicol-resistant variant of P2 (ref. 28; Supplementary Tables 1 and 2), a large conjugative plasmid of *S.* Typhimurium SL1344
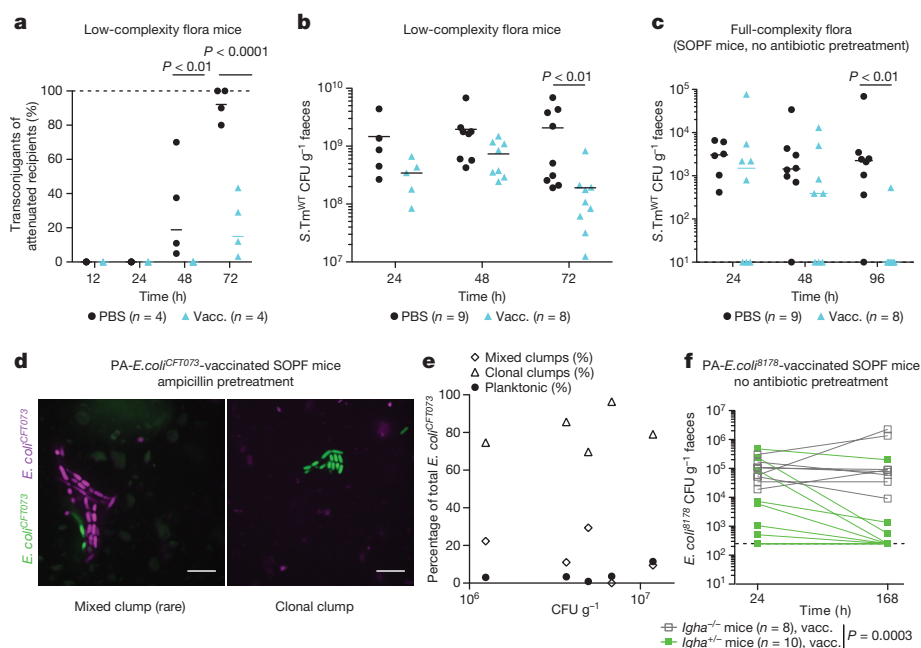
Figure 3 | Enchained growth inhibits conjugative plasmid transfer.
a, Mock- (PBS/irrelevant vaccine) or PA-S.Tm- (vacc.) vaccinated mice were sequentially infected with 10^2 CFU of SL1344 carrying a modified P2 plasmid (P2$_{cat}$ donor), immediately followed by 10^2 CFU of recipient (14028) S. Typhimurium. The percentage transconjugants of total 14028 S. Typhimurium. Repeat-measured ANOVA with Bonferroni post hoc tests ($n = 5$ (PBS) $n = 7$ (vacc.)). **b**, *In vitro* plasmid transfer over 60 min (10^9 CFU ml^{-1}) in the presence or absence of bacterial coating with murinized monoclonal dimeric IgA against the S. Typhimurium O-antigen (mSTA121 60 μg ml^{-1}). $n = 5$ independent experiments. Mann–Whitney U-test.

(10^2 CFU each, by gavage). Vaccine-induced IgA bound equally to both S. Typhimurium strains (Extended Data Fig. 10a–c). Vaccination decreased the rates of plasmid transfer *in vivo* (Fig. 3a, Extended Data Fig. 10d–f). *In vitro* data at high donor and recipient densities

precluded a direct inhibitory effect of IgA on conjugation (Fig. 3b), and flagella-driven motility was dispensable for efficient conjugation in the mouse gut (Extended Data Fig. 10g–i). Therefore, the reduced conjugation efficiency in vaccinated mice is probably attributable to IgA-mediated enchainment of donor and recipient clones into separate clumps.

In the streptomycin mouse model, microbiota are suppressed and final S. Typhimurium densities are 10–100-fold higher than in natural infections[5], sufficiently high that classical agglutination co-exists with enchained growth (Fig. 1j, Extended Data Figs 6, 7). In other words, the streptomycin mouse model exaggerates the contribution of classical agglutination. This promotes conjugation and may explain why even vaccinated mice show appreciable plasmid transfer at late time points ($\geq$48 h after infection; Fig. 3a). We therefore repeated the plasmid transfer experiment in mice with intact 'low-complexity flora'[8,26,29], without antibiotic pretreatment. Mice with low-complexity flora allow moderate levels of S. Typhimurium colonization, such that IgA predominantly acts through enchained growth. In this setting, high-avidity IgA can block plasmid transfer up to day 3 after infection (Fig. 4a, Extended Data Fig. 10j–l). Thus, enchained growth is even more prominent when pathogen densities remain moderate. In the absence of antibiotics, the intact microbiota can compete more efficiently with S. Typhimurium, promoting its clearance from the gut lumen. Correspondingly, high-avidity IgA enhanced the elimination of S. Typhimurium from the gut lumen of mice that had an intact low- or full-complexity flora (Fig. 4b, c).

This reveals a previously overlooked function of IgA. Vaccine-induced high-avidity IgA accelerates pathogen elimination from the gut and could slow bacterial adaptation in the gut lumen by driving

Figure 4 | Enchained growth functions effectively at realistic, low pathogen densities, and can be observed for other bacterial species.
a, Low-complexity flora mice[8,26,29] were mock- or PA-S.Tm- (vacc.) vaccinated and sequentially infected with 10^2 CFU of the P2$_{cat}$-carrying attenuated donor strain (SL1344 S. Typhimurium), immediately followed by 10^2 CFU of the attenuated recipient strain (14028 S. Typhimurium) ($n = 4$). Repeat-measures ANOVA with Bonferroni post hoc tests, two representative experiments of three are shown. **b**, Total S.Tm^{WT} loads in faeces of mock- and PA-S.Tm-vaccinated mice with low-complexity flora that were infected with 10^5 CFU. Repeat-measured ANOVA on log-normalized data with Bonferroni post hoc tests. **c**, Mock- or PA-S. Tm-vaccinated mice (specific opportunistic pathogen free (SOPF)) were

challenged with 10^5 CFU S.Tm^{WT} (without antibiotic pretreatment) and faecal CFU were determined until day 4 after infection (median and individual values shown). **d**, **e**, Peracetic-acid-inactivated E. $coli^{CFT073}$-vaccinated wild-type mice (PA-E. $coli^{CFT073}$) were pretreated with ampicillin and infected with 10^5 CFU of a 1:1 ratio of E. $coli^{CFT073}$ constitutively expressing mCherry (red) or GFP (green). Representative images of explanted caecal content (**d**) and quantification of clump clonality (**e**) from confocal micrographs ($n = 5$). Scale bar, 10 μm.
f, $Igha^{-/-}$ (open symbols, grey) and littermate $Igha^{+/-}$ (closed symbols, green) SOPF mice were vaccinated with a PA-E. $coli^{8178}$ strain. On day 21, all mice received 10^5 CFU E. $coli^{8178}$ by gavage, without antibiotic pretreatment. Faecal CFU were analysed at the indicated time points. Repeat-measures ANOVA on log-normalized data, $P = 0.0003$.

clonal extinction and preventing horizontal gene transfer. The presence of an intact microbiota enhances this effect by maintaining lower *S.* Typhimurium densities and providing competition.

IgA-mediated enchained growth may be of general importance for enteric bacteria. Supporting this view are observations of enchained growth and IgA-driven clearance from the gut lumen of other pathogens and commensals (for example, *Escherichia coli* strains CFT073 and 8178; Fig. 4d–f). Furthermore, in contrast to classical agglutination, which is restricted to high-density colonization, enchained growth dominates in all situations in which the bacterial targets are rare and growing (Fig. 1i–k, Extended Data Figs 6, 7), for example, in bacterial food poisoning[4] or pathobiont-fuelled disease in dysbiosis[9,30]. If high bacterial densities are reached, classical agglutination and enchained growth can complement each other in protection of the mucosa against invasion from abundant growing bacteria (Fig. 1i–k, Extended Data Figs 6, 7).

Finally, enchained growth explains how IgA-mediated cross-linking of bacteria, without any additional immune activation or bactericidal activity, can beneficially control bacteria in the intestine. The selective disadvantage of IgA-driven clumping and the flow of intestinal contents are sufficient to disarm and clear antibody-targeted bacteria, on the basis of the pathogenicity-associated behaviour of fast growth. Enchained growth thus avoids collateral damage to the host and promotes competitive resilience of the normal microbiota. This is particularly powerful for pathogens such as non-typhoidal *Salmonella* spp. that actively benefit from intestinal inflammation for microbiota suppression[27–29]. Our work predicts that IgA-mediated enchained growth is an important mechanism of protecting the intestinal ecosystem, and could be harnessed, through oral vaccination, to decelerate the evolution and spread of antimicrobial resistance.

1. Mantis, N. J., Rol, N. & Corthésy, B. Secretory IgA's complex roles in immunity and mucosal homeostasis in the gut. *Mucosal Immunol.* **4,** 603–611 (2011).
2. Pabst, O. New concepts in the generation and functions of IgA. *Nat. Rev. Immunol.* **12,** 821–832 (2012).
3. Slack, E., Balmer, M. L. & Macpherson, A. J. B cells as a critical node in the microbiota–host immune system network. *Immunol. Rev.* **260,** 50–66 (2014).
4. WHO. Risk assessments of *Salmonella* in eggs and broiler chickens. http://www.who.int/foodsafety/publications/micro/salmonella/en/ (2002).
5. Gopinath, S., Carden, S. & Monack, D. Shedding light on *Salmonella* carriers. *Trends Microbiol.* **20,** 320–327 (2012).
6. White, P. B. Further Studies of the *Salmonella* Group. *Great Britain Medical Research Council (Her Majesty's Stationary Office)* **103,** 3–160 (1926).
7. Le Minor, L. & Popoff, M. Y. *Kauffmann–White-Scheme* (Behring Diagnostika, 1988).
8. Endt, K. *et al.* The microbiota mediates pathogen clearance from the gut lumen after non-typhoidal *Salmonella* diarrhea. *PLoS Pathog.* **6,** e1001097 (2010).
9. Hendrickx, A. P. *et al.* Antibiotic-driven dysbiosis mediates intraluminal agglutination and alternative segregation of *Enterococcus faecium* from the intestinal epithelium. *MBio* **6,** e01346e15 (2015).
10. Levinson, K. J., De Jesus, M. & Mantis, N. J. Rapid effects of a protective O-polysaccharide-specific monoclonal IgA on *Vibrio cholerae* agglutination, motility, and surface morphology. *Infect. Immun.* **83,** 1674–1683 (2015).
11. Kiørboe, T. *A mechanistic approach to plankton ecology.* (Princeton Univ. Press, 2008).
12. van Schothorst, M. & Beckers, H. J. Persistent excretion of salmonellas. *BMJ* **2,** 1301 (1978).
13. Forbes, S. J., Eschmann, M. & Mantis, N. J. Inhibition of *Salmonella enterica* serovar Typhimurium motility and entry into epithelial cells by a protective antilipopolysaccharide monoclonal immunoglobulin A antibody. *Infect. Immun.* **76,** 4137–4144 (2008).
14. Forbes, S. J. *et al.* Association of a protective monoclonal IgA with the O antigen of *Salmonella enterica* serovar Typhimurium impacts type 3 secretion and outer membrane integrity. *Infect. Immun.* **80,** 2454–2463 (2012).
15. Amarasinghe, J. J., D'Hondt, R. E., Waters, C. M. & Mantis, N. J. Exposure of *Salmonella enterica* serovar Typhimurium to a protective monoclonal IgA triggers exopolysaccharide production via a diguanylate cyclase-dependent pathway. *Infect. Immun.* **81,** 653–664 (2013).
16. Michetti, P., Mahan, M. J., Slauch, J. M., Mekalanos, J. J. & Neutra, M. R. Monoclonal secretory immunoglobulin A protects mice against oral challenge with the invasive pathogen *Salmonella typhimurium. Infect. Immun.* **60,** 1786–1792 (1992).
17. Michetti, P. *et al.* Monoclonal immunoglobulin A prevents adherence and invasion of polarized epithelial cell monolayers by *Salmonella typhimurium. Gastroenterology* **107,** 915–923 (1994).
18. Barthel, M. *et al.* Pretreatment of mice with streptomycin provides a *Salmonella enterica* serovar Typhimurium colitis model that allows analysis of both pathogen and host. *Infect. Immun.* **71,** 2839–2858 (2003).
19. Kaiser, P., Diard, M., Stecher, B. & Hardt, W. D. The streptomycin mouse model for *Salmonella* diarrhea: functional analysis of the microbiota, the pathogen's virulence factors, and the host's mucosal immune response. *Immunol. Rev.* **245,** 56–83 (2012).
20. Hapfelmeier, S. *et al.* The *Salmonella* pathogenicity island (SPI)-2 and SPI-1 type III secretion systems allow *Salmonella* serovar Typhimurium to trigger colitis via MyD88-dependent and MyD88-independent mechanisms. *J. Immunol.* **174,** 1675–1685 (2005).
21. Moor, K. *et al.* Peracetic acid treatment generates potent inactivated oral vaccines from a broad range of culturable bacterial species. *Front. Immunol.* **7,** 34 (2016).
22. Kaiser, P., Slack, E., Grant, A. J., Hardt, W. D & Regoes, R. R. Lymph node colonization dynamics after oral *Salmonella typhimurium* infection in mice. *PLoS Pathog.* **9,** e1003532 (2013).
23. Perfeito, L., Fernandes, L., Mota, C. & Gordo, I. Adaptive mutations in bacteria: high rate and small effects. *Science* **317,** 813–815 (2007).
24. Barlow, M. Methods in Molecular Biology. *Horizontal Gene Transfer* **532,** 397–411 (2009).
25. Grant, A. J. *et al.* Modelling within-host spatiotemporal dynamics of invasive bacterial disease. *PLoS Biol.* **6,** e74 (2008).
26. Maier, L. *et al.* Granulocytes impose a tight bottleneck upon the gut luminal pathogen population during *Salmonella typhimurium* colitis. *PLoS Pathog.* **10,** e1004557 (2014).
27. Stecher, B. *et al. Salmonella enterica* serovar typhimurium exploits inflammation to compete with the intestinal microbiota. *PLoS Biol.* **5,** 2177–2189 (2007).
28. Stecher, B. *et al.* Gut inflammation can boost horizontal gene transfer between pathogenic and commensal Enterobacteriaceae. *Proc. Natl Acad. Sci. USA* **109,** 1269–1274 (2012).
29. Stecher, B. *et al.* Like will to like: abundances of closely related species can predict susceptibility to intestinal colonization by pathogenic and commensal bacteria. *PLoS Pathog.* **6,** e1000711 (2010).
30. Palm, N. W. *et al.* Immunoglobulin A coating identifies colitogenic bacteria in inflammatory bowel disease. *Cell* **158,** 1000–1010 (2014).

METHODS

Ethics statement. All animal experiments were approved by the legal authorities (licenses 223/2010, 222/2013 and 193/2016; Kantonales Veterinäramt Zürich, Switzerland) and performed according to the legal and ethical requirements.

Mice. Unless otherwise stated, all experiments used recently re-derived SOPF C57BL/6 mice. VilRFP (B6.B6-Gt(ROSA)26Sortm1Hjf × B6.SJL-Tg(Vil-cre)997Gum/J)[31], 129S6/SvEvTac, $Igha^{-/-}$ (ref. 32), $Pigr^{-/-}$ (ref. 33), Igh-$J^{-/-}$ (all C57BL/6 background) were recently re-derived into a specific opportunistic pathogen-free (SOPF) foster colony to normalize the microbiota and bred under full barrier conditions in individually ventilated cages in the ETH Phenomics centre (EPIC, RCHCI), ETH Zürich. Low-complexity flora mice (C57BL/6) are ex-germfree mice, which were colonized with a naturally diversified Altered Schaedler flora in 2007[29,34] and were bred in individually ventilated cages under strict hygienic isolation in Rodent Center at ETH. Vaccinations were started between 5 and 6 weeks of age.

Data reporting. As strong phenotypes were expected, no statistical methods were used to predetermine sample size. Instead, we adhered to the standard practice of analysing at least 5 mice per group, pooled from 2 or more independent experiments. Males and females were randomized between groups to obtain identical ratios wherever possible. The investigators were not blinded to allocation during experiments and outcome assessment.

Bacterial strains and growth conditions. Unless otherwise stated, for infection experiments, wild-type *Salmonella enterica* serovar *enterica* Typhimurium (SL1344 wild-type clone SB300) or the respective mutants were cultured in Lysogeny broth (LB) containing the appropriate antibiotics for 12 h at 37 °C, diluted 1:20 and sub-cultured for 3 h in 0.3 M NaCl supplemented LB without antibiotics[18].

The attenuated recipient is the product of two P22 transductions (*invG::cat*, *ssaV::kan*) into the 14028S strain, followed by flipping out of the antibiotic resistance cassettes by the flipase encoded on pCP20. The *lpfED::aphT* tag was added by P22 transduction[35]. The recipient strain carrying the *fliGHI*::Tn*10* is the result of P22 transduction of (*fliGHI*::Tn*10*) into 14028S.

All bacterial strains used in this study are listed in Supplementary Table 1[36–42].

Plasmids used in this study. All plasmids used in this study are listed in Supplementary Table 2 refs 43, 44). The pBADGFPmut2 plasmid was constructed by insertion of a EcoRI gfp-mut2 fragment from pM979 (ref. 38) into pBAD24, digested by EcoRI (Fermentas) and dephosphorylated (shrimp alkaline phosphatase, NEB).

Production of peracetic-acid-killed vaccines. Peracetic-acid-killed vaccines were produced as described in ref. 21. Briefly, bacteria were grown overnight to late stationary phase, collected by centrifugation and resuspended to a density of 10^9–10^{10} per ml in sterile PBS. Peracetic acid (Sigma-Aldrich) was added to a final concentration of 1%. The suspension was mixed thoroughly and incubated for 60 min at room temperature. Bacteria were washed once in 40 ml of sterile 10× PBS and subsequently three times in 50 ml sterile 1× PBS. The final pellet was resuspended to yield a density of 10^{11} particles per ml in sterile PBS (determined by optical density (OD$_{600}$)) and stored at 4 °C for up to three weeks. As a quality control, each batch of vaccine was tested before use by inoculating 100 μl of the killed vaccine (one vaccine dose) into 300 ml LB and incubating over night at 37 °C with aeration. Vaccine lots were released for use only when a negative enrichment culture had been confirmed.

Oral vaccination with peracetic-acid-killed vaccines. Mice were vaccinated as previously described[21]. Briefly, mice received 10^{10} particles of the respective peracetic-acid-killed bacteria in PBS by oral gavage once per week for three weeks. On day 21 after the first gavage, mice were used for infection experiments.

Challenge infections with *S.* Typhimurium. All infections were performed in individually ventilated cages at the RCHCI, Zurich as described previously[18]. Unless otherwise stated, mice were pretreated with either 1 g kg^{-1} streptomycin sulphate or 0.8 g kg^{-1} ampicillin sodium salt in sterile PBS by gavage. 24 h later, the mice were inoculated with the indicated CFU and strain by gavage. For determination of total bacterial loads, fresh faecal pellets, mesenteric lymph nodes, spleen and caecal content were subjected to bead-beating and plated on MacConkey agar plates containing 50 μg ml^{-1} streptomycin.

For conjugative pCol1B9 (P2$_{cat}$) plasmid transfer experiments, ampicillin-pretreated SOPF C57BL/6 mice or untreated low-complexity flora mice were sequentially infected with equal inocula of donor and recipient strains (at 10^2 CFU each) (Supplementary Tables 1 and 2). Both strains were carrying additional plasmids conferring resistance to ampicillin and coding for fluorescence proteins (conditional expression (pM975), or constitutive expression (pM965 and pFPV25.1)). Faecal densities of donors, recipients and transconjugants were evaluated by selective plating (MacConkey agar plates containing 50 μg ml^{-1} kanamycin, 6 μg ml^{-1} chloramphenicol or combinations thereof).

Determination of bacterial growth rates in the gut lumen. pAM34 is a vector in which the replication primer promoter is under the control of the LacI repressor such that plasmid replication only occurs in the presence of isopropyl β-D-1-thiogalactopyranoside (IPTG)[44]. *S.*Tm^{att} carrying the pAM34 plasmid was therefore cultured overnight in the presence of 1 mM IPTG in LB and in the absence of antibiotics, to avoid selection of IPTG-independence. Subsequently, the culture was diluted 1:20 into fresh LB and cultured at 37 °C for 3 h. The inocula were prepared by centrifugation of sufficient culture to give the desired CFU and resuspended in 50 μl of sterile PBS. SOPF C57BL/6 mice that had received 1 g kg^{-1} streptomycin per os (p.o.) 24 h previously, were infected orally with either 10^3, 10^5 or 10^7 CFU of the pAM34-carrying inoculum. Simultaneously, the inoculum was serially diluted into LB without IPTG and cultured overnight to determine the relationship between bacterial generations and plasmid loss for each experiment. pAM34 carriage was determined by plating faeces and overnight cultures on MacConkey agar plates containing 50 μg ml^{-1} streptomycin only (total CFU) or 100 μg ml^{-1} ampicillin and 1 mM IPTG (pAM34-carrying CFU). The overnight culture total CFU and inoculum CFU were used to calculate fold expansion, and therefore generation number (assuming zero death) for each sample. This was plotted against the log$_2$ of the fraction of pAM34-carrying bacteria and linear regression carried out to determine the relationship between plasmid loss and generations. The copy number of the plasmid is equivalent to $2^{(\text{intercept} - \log_2(100))}$, as there is no production of plasmid-negative bacteria until the mean plasmid copy number has been diluted to close to $n = 1$ per cell. The equation derived by linear regression was then used to back-calculate bacterial generations between the inoculum and faecal bacteria and least-squares linear regression used to calculate the maximum growth rate *in vivo*.

Quantification of faecal lipocalin-2. Faecal pellets collected at the indicated time points were homogenized in PBS by bead-beating at 25 Hz, for 1 min. Large particles were sedimented by centrifugation at 300*g*, 1 min. The resulting supernatant was then analysed in serial dilution using the mouse lipocalin-2 ELISA duoset (R&D) according to the manufacturer's instructions.

Analysis of IgA-coating of *S.* Typhimurium in caecal content. Fresh caecal content was resuspended in sterile PBS by bead-beating at 25 Hz, 1 min. An aliquot estimated to contain no more than 10^6 *S.* Typhimurium was directly stained with a monoclonal human IgG-anti-O12 (STA5, see below) and biotin-conjugated anti-mouse IgA clone RMA-1 (Biolegend). After washing, secondary reagents Alex647-tagged anti-human IgG (Jackson Immunoresearch) and Pacific-Blue-conjugated streptavidin (Molecular Probes) were added. After a final washing step, samples were analysed on a BD LSRII flow cytometer with settings adapted for optimal detection of bacterial-sized particles. The median fluorescence intensity of IgA staining on *S.* Typhimurium was determined by gating on O12-positive events in FlowJo (Treestar).

Analysis of specific antibody titres by bacterial flow cytometry. Specific antibody titres in mouse intestinal washes were measured by flow cytometry, as previously described[45]. Briefly, intestinal washes were collected by flushing the small intestine with 5 ml PBS, centrifuged at 16,000*g* for 30 min and aliquots of the supernatants were stored at −20 °C until analysis. Bacterial targets (antigen against which antibodies are to be titrated) were grown to late stationary phase and gently pelleted for 2 min at 3,000*g*. The pellet was washed with sterile-filtered FACS buffer before resuspending at a density of approximately 10^7 bacteria per ml. After thawing, intestinal washes were centrifuged again at 16,000*g* for 10 min. Supernatants were used to perform serial dilutions. 25 μl of the dilutions were incubated with 25 μl bacterial suspension at 4 °C for 1 h. Bacteria were washed twice with 200 μl FACS buffer before resuspending in 25 μl FACS buffer containing monoclonal FITC-tagged anti-mouse IgA (BD Pharmingen, 10 μg ml^{-1}). After 1 h of incubation, bacteria were washed once with FACS buffer and resuspended in 300 μl FACS buffer for acquisition on FACS LSRII using FSC and SSC parameters in logarithmic mode. Data were analysed using FloJo (Treestar). After gating on bacterial particles, log-median fluorescence intensities (MFI) were plotted against antibody concentrations for each sample and four-parameter logistic curves fitted using Prism (Graphpad). Titres were calculated from these curves as the inverse of the antibody concentration, giving an above-background signal. To estimate the absolute concentration of specific antibodies, the dilution factor required to give above-background staining was calculated as above, and compared to that of a specific mouse monoclonal dimeric IgA (mSTA121) of known concentration.

Production of monoclonal human IgA and IgG and murinized monoclonal IgA. Memory B cells were isolated from cryopreserved peripheral blood mononuclear cells by magnetic cell sorting with anti-CD22-FITC antibodies (BD Pharmingen) and anti-FITC microbeads (Miltenyi Biotec), followed by flow cytometry sorting. The B cells were immortalized with Epstein–Barr virus (EBV) in the presence CpG-DNA (2.5 μg ml^{-1}) and irradiated feeder cells, as described previously[46]. Two weeks after immortalization, culture supernatants were tested for binding to formaldehyde-treated heat-inactivated *S.* Typhimurium cells by ELISA and FACS analysis as above. STA5 supernatant containing IgG against *S.* Typhimurium O-antigen was filtered and used directly. To generate murinized monoclonal IgA, cDNA was synthesized from the mSTA121-positive culture and both heavy chain and light chain variable regions were sequenced. The mouse IgA heavy chain

and J chain were synthesized with reference to the IMGT database. mSTA121 monoclonal antibody was produced recombinantly as mouse dimeric IgA by transient transfection of HEK 293 Freestyle Cells (Invitrogen) using polyethylenimine (PEI), and purified by antibody affinity chromatography (CaptureSelect LC-lambda (Hu) Affinity Matrix, Thermo Fisher Scientific).

Purification of intestinal IgA for *in vitro* assays. Small intestinal lavages from mice that were either vaccinated with PA-*S*.Tm or PBS only, were collected as described above and stored at −80 °C until usage. Intestinal lavages were thawed and centrifuged at 16,000g for 10 min. The supernatants were diluted in LB media, sterile filtered (0.22-μm filter) and loaded onto a 100 kDa cut-off filter column (Amicon Ultra UFC910096). The columns were centrifuged at 6,340g for 1 h (Heraeus Megafuge 1.0 R) and the flow through was discarded. The collected liquid was resuspended in 0.5 ml LB medium per 2 ml starting intestinal lavage.

***In vitro* growth assays in the presence of specific- and control-IgA.** *S*. Typhimurium carrying an arabinose-inducible GFP on the plasmid pBADGF-Pmut2 (pZ1603) were grown overnight in LB containing 100 μg ml^{-1} ampicillin. The overnight culture was diluted 1:100 in LB with ampicillin (100 μg ml^{-1}) and 1% w/v arabinose, and subcultured for 3 h to fully induce the reporter. Subsequently bacteria were thoroughly washed and diluted into LB supplemented with purified intestinal IgA (3 mg ml^{-1} total IgA) from the indicated source. Samples were analysed by plating for total CFU determination and flow cytometry for GFP dilution, as described previously[47].

For competitive growth, *S*. Typhimurium and *S*. Enteritidis were grown separately overnight in LB supplemented with the respective antibiotics. The *S*. Typhimurium and *S*. Enteritidis cultures were mixed 1:1 and diluted 1:100 into LB without antibiotics, supplemented with purified intestinal IgA at 3 mg ml^{-1}. Approximately 10^4–10^5 CFU of the *S*. Typhimurium/*S*. Enteritidis mix were added to a 96-well plate (TPP 92096) and bacteria were incubated at 37 °C without agitation. Every hour, the top half of the bacterial culture was removed and fresh LB supplemented with purified IgA was added to maintain saturating levels during growth. Samples were collected every 0.5–1 h for plating and FACS analyses. IgA coating was verified by flow cytometry. Before plating on selective LB agar and analysis by bacterial flow cytometry, the bacterial culture was bead-beaten at 25 s^{-1} for 1 min to disrupt aggregates.

Fluorescence microscopy of fixed caeca. Whole caeca were fixed in PBS 4% paraformaldehyde/4% sucrose, saturated in PBS/20% sucrose, embedded in OCT (optimum cutting temperature medium; Tissue-Tek), flash-frozen, and stored at −80 °C. 10–20-μm cryosections were air-dried, rehydrated in PBS for 1 min, permeabilized in PBS/0.5% Triton X-100 for 3 min, and blocked in PBS/10% normal goat serum for ≥15 min. Sections were incubated with the indicated antibodies for ≥15 min each, washed with PBS, and mounted with Mowiol (Calbiochem). For quantification of *S*. Typhimurium in tissue, 20 μm cross-sections were stained with anti-ICAM-1/CD54 (clone 3E2, Becton Dickinson), anti-hamster-Cy3 (Jackson), AlexaFluor647-conjugated phalloidin (Molecular Probes), and DAPI (Sigma Aldrich). Tissue-residing *S*. Typhimurium were identified by expression of the P*ssaG-GFPmut2* reporter, and were enumerated at 40−100-fold magnification, as previously described[48] by an investigator blinded to sample identity. Data presented are mean values of 6–9 non-consecutive tissue sections per mouse. For quantification of *S*. Typhimurium in the caecal lumen, 10-μm cross-sections were stained with rabbit antibody against *S*. Typhimurium LPS (antigen group B factor 4-5; Difco), anti-rabbit-Cy3 or anti-rabbit-Cy5 (both from Jackson) and DAPI. Imaging was peformed using a Zeiss Axiovert 200m microscope with a 100× oil-objective, a spinning disc confocal laser unit (Visitron), and two Evolve 512 EMCCD cameras (Photometrics). Post-capture processing and analysis employed Visiview (Visitron) and ImageJ.

To quantify the 'infectious population size', the number of single and paired bacteria was determined on the basis of the *S*. Typhimurium LPS staining. 10 high-power fields containing non-aggregated bacteria per PA-*S*.Tm-vaccinated mouse were scored.

Live confocal microscopy of caecal content. Vaccinated or control mice were pretreated with 0.8 g kg^{-1} ampicillin sodium salt in sterile PBS. 24 h later, mice received 10^7 CFU of a 1:1 mix of *S*.Tm^{att} or *E*. *coli*^{CFT073} expressing mCherry (pFPV25.1) and GFP (pM965). For imaging, caecal content was collected and diluted gently at 1:10 w/v in sterile PBS containing 6 μg ml^{-1} chloramphenicol to prevent growth during imaging. 200 μl of the suspension were transferred to an 8-well Nunc Laboratory-Tek Chambered Coverglass (Thermo Scientific) and imaged at 100× using the Zeiss Axiovert 200-m microscope. To determine the distribution of bacteria in aggregates, $n = 25$ high-power fields per mouse were randomly selected and imaged for mCherry and GFP fluorescence. The images were merged in ImageJ and individual bacteria scored visually as either planktonic, present in a single-colour aggregate or present in a mixed aggregate of a given size.

To determine *S*. Typhimurium motility, ampicillin-pretreated mice were infected with 10^5 CFU *S*.Tm^{att} (pM965) for 18 h. Caecal content was gently diluted

1:10 w/v in sterile PBS. The heating chamber of the microscope was set to 37 °C and all images were taken with an exposure time of 1 s. Swimming distances were determined by measuring individual bacterial trajectories in ImageJ 64-bit.

Quantifying 'randomness' of cluster composition. Confocal micrographs of live caecal content were subjected to cell segmentation and classification into red (mCherry$^+$) and green (GFP$^+$) types has been performed with ilastik software, version 1.2, for supervised pixel- and object-level classification[49]. All subsequent analysis was carried out in MATLAB (The Mathworks, Inc.). Visually inspecting the clusters in all images indicated that pairs with a centre-to-centre separation of less than 6 μm were typically part of the same cluster. For each animal and across all images, we therefore detected cell pairs (mCherry$^+$–mCherry$^+$, mCherry$^+$–GFP$^+$, and GFP$^+$–GFP$^+$) with centre-to-centre separation that was smaller than 6 μm (50 pixels). We then randomly re-coloured the cells in the images (mCherry$^+$ assigned to each cell with a probability equal to the fraction of mCherry$^+$ cells observed for each animal), and recalculated the number of observed pairs in each of the three categories.

By iterating this procedure 1,000 times, we generated distributions of the expected fraction of clumped mCherry$^+$–mCherry$^+$ cell pairs over the total number of cell pairs if the location of red cells was random. We then determined the probability of observing the measured fraction of clustered mCherry$^+$ cells.

Measuring *S*. Typhimurium cell size. Cell size was measured on the basis of fluorescence microscopy images using a custom script in MATLAB (The Mathworks, Inc.). First, cells were recognized as particles on the basis of fluorescence intensity. Second, the resulting binary images were visually compared to the original images to check whether cells were correctly recognized. Third, pixel-lengths for long and short axes of all recognized cells were extracted using the regionprops function, and converted to micrometers using the objective-specific conversion factor 0.128 μm per pixel. The mean values of long axes lengths were used for further analysis.

Intravital two-photon microscopy. Intravital microscopy was performed similarly to previously published[31]. Briefly, anaesthetized, intubated mice were artificially ventilated with oxygen containing 1.8–1.9% isoflurane. After exposing the caecum and submerging it in ringer/lactate solution, images were acquired using a Leica SP8 DMI6000B microscope equipped with a HC PL IRAPO 403/1.10 water immersion objective, emission filters for GFP (525/50) and mCherry (RFP) (585/40), and nondescanned Hybrid detectors (Leica). GFP and mCherry was excited using a two-photon MaiTai XF Laser (Spectra-Physics) tuned to 920 nm (pulsed at 80 MHz with pulse width <80 fs). The microscope was operated using the Leica application suite at ScopeM (ETHZ). The distance measurement was performed using the orthogonal view function of Fiji (based on ImageJ 1.49h). Z distance was 7.5 μm per section. For measurement of the location of 25 μm beads, 10 μl of 25 μm YG latex beads (Polysciences) were injected directly into the caecal lumen of an intubated mouse and were allowed to equilibrate for 30 min. The tissue was sealed using Histoacryl glue (B. Braun) and imaged as described above.

***In vitro* plasmid transfer.** Overnight cultures of P2$_{cat}$ wild-type donor and wild-type recipient were diluted 1:50, and subcultured for 4 h in LB without antibiotics. The resulting cultures were washed with PBS. 45 μl of donor and recipient PBS-washed subcultures were separately incubated with 60 μg ml^{-1} of monoclonal dimeric IgA specific for the *S*. Typhimurium O-antigen (mIgA STA121) for 5 min at room temperature. P2$_{cat}$ wild-type donor and wild-type recipient strains were then mixed and loaded onto a 0.025 μm MF-Millipore mixed cellulose ester membrane using a syringe. Membranes were placed on LB agar without antibiotics and incubated for 1 h at 37 °C. Membranes were then each bead-beaten in 1 ml PBS at 25 Hz for 1 min. Resuspended mixtures were diluted and plated on selective MacConkey agar plates. IgA coating was confirmed by bacterial flow cytometry as described above.

Basic statistics. Where two groups were compared, Mann–Whitney U non-parametric tests were employed. Where more than two groups were compared, Kruskal–Wallis tests with Dunn's post hoc tests were used to correct for multiple testing. Where time-courses were compared with two different groups, data was transformed to approximate a normal distribution and repeat-measures ANOVA was used to determine significance.

Mathematical modelling. *Modelling of translocation to the mLN.* Experimental data was generated as described previously[22], using seven wild-type isogenic tagged strain (WITS) tags[25] at 1:35 of the total 10^5 CFU inoculum. At this dilution, more than 2,500 clones of each WITS reach the caecal lumen of vaccinated mice, well above the stochastic limit for clonal extinction in the gut lumen. The distribution of WITS-tagged strains reaching the mLN was quantified by plating, enrichment culture and qPCR as described[22]. This distribution was then used to parameterize a stochastic birth–death process modified by immigration, describing mLN colonization[22]. Parameter optimization generated the number of translocations from the gut lumen to the mLN per day (μG) and the net replication rate (that is, replication minus clearance) in the mLN ($r - c$).

The number of translocations per day is in fact the product of G (the size of the infectious gut luminal population) and μ (the translocation rate per infectious

luminal bacterium). If we assume that μ takes the same value in the vaccinated and naive case (that is, we use the predicted distribution of μ calculated in naive mice: mean $\mu_{naive} = 1.06 \times 10^{-7}$), we can estimate a distribution for G by simple division of the total daily translocation rate (that is, μG) by μ_{naive}, bootstrapping over 1,000 randomly sampled values from the predicted normal distributions.

To estimate μ directly for the vaccinated case, we employed a bootstrapping protocol over 10^6 randomly sampled values from the expected normal distributions of G (determined by plating of caecal content and microscopic determination of the percentage planktonic *S.* Typhimurium) and μG (determined from this stochastic model). Of note, the resulting distribution is non-normal and the output is therefore analysed using non-parametric statistics.

Calculating and modelling clonal loss from the caecal lumen. Vaccinated and naive mice were infected with either 10^5 CFU or 10^{10} CFU *S.*Tm[att], spiked with an average of 10 copies of each of seven *S.*Tm[att] WITS strains. WITS frequencies were determined by plating, enrichment culture and qPCR as described previously[22,25]. The loss of evenness was calculated as described previously, on the basis of the cumulative sum of the WITS proportions[26].

To estimate the effect of enchained growth on clonal loss, we simulated a simple scenario on the basis of the experiment described in Fig. 2a–c. There are three important parameters for the dynamics of the bacterial population:

(1) Probability to seed the caecum: we assume that there is a probability P for each bacteria in the 10^5 inoculum to establish in the caecum. In the case of the mock-vaccinated mice, clonal loss can be mainly attributed to this initial bottleneck, as subsequent bacterial loss is a small effect compared to the division rate. Based on the experimental data, we estimate the probability to lose a given barcode, given their frequency in the inoculum, as $P = 0.115$.
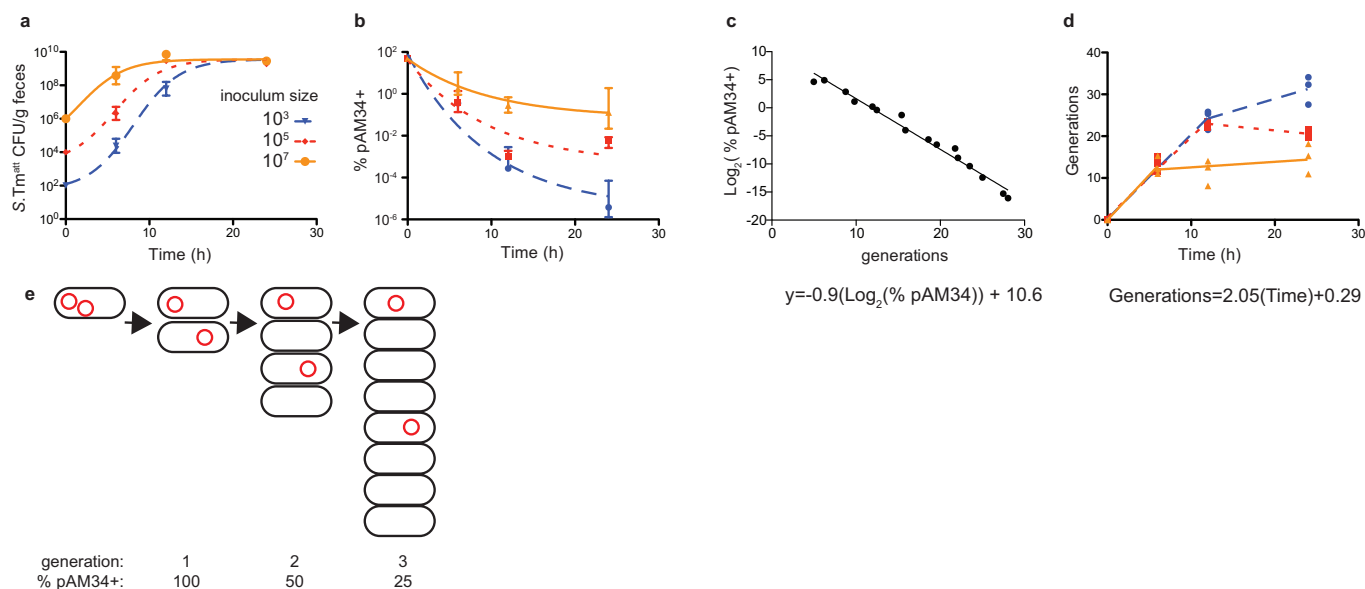
(2) Growth kinetics in the caecal lumen: based on Extended Data Fig. 1. When streptomycin pretreated mice are infected with 10^5 CFU *S.* Typhimurium, bacteria divide twice per hour until 12 h after infection, when they reach the caecal carrying capacity and net growth stops (that is, the growth rate equals the clearance rate).

(3) Kinetics of clearance in the faecal stream: to maintain faeces production, approximately 10% of the caecal content is cleared to the colon and lost in the faeces every 15 min.

The simulation starts from the number of barcoded bacteria in the inoculum. These bacteria establish in the caecum through a Poisson process with a probability P. We reasonably assume that the established bacteria become equally distributed in the caecal content by peristaltic mixing and that the untagged bacteria have no effect on the barcoded clonal distribution. We simulate the established barcoded bacterial growth deterministically as in point (2) above; and random loss, with a probability 10% every 15 min (point (3) above). We simulated the two extreme cases: no enchained growth ($\delta = 1$), where δ is the probability of escaping enchained growth, or a 'perfect' enchained growth, where individual clones never segregate, meaning that bacteria get eliminated in the faeces in perfect clonal clusters ($\delta = 0$). For $\delta = 1$, we simply track the number of bacteria, whereas for $\delta = 0$, we track the number of clones. We then compute the evenness, as in ref. 26.
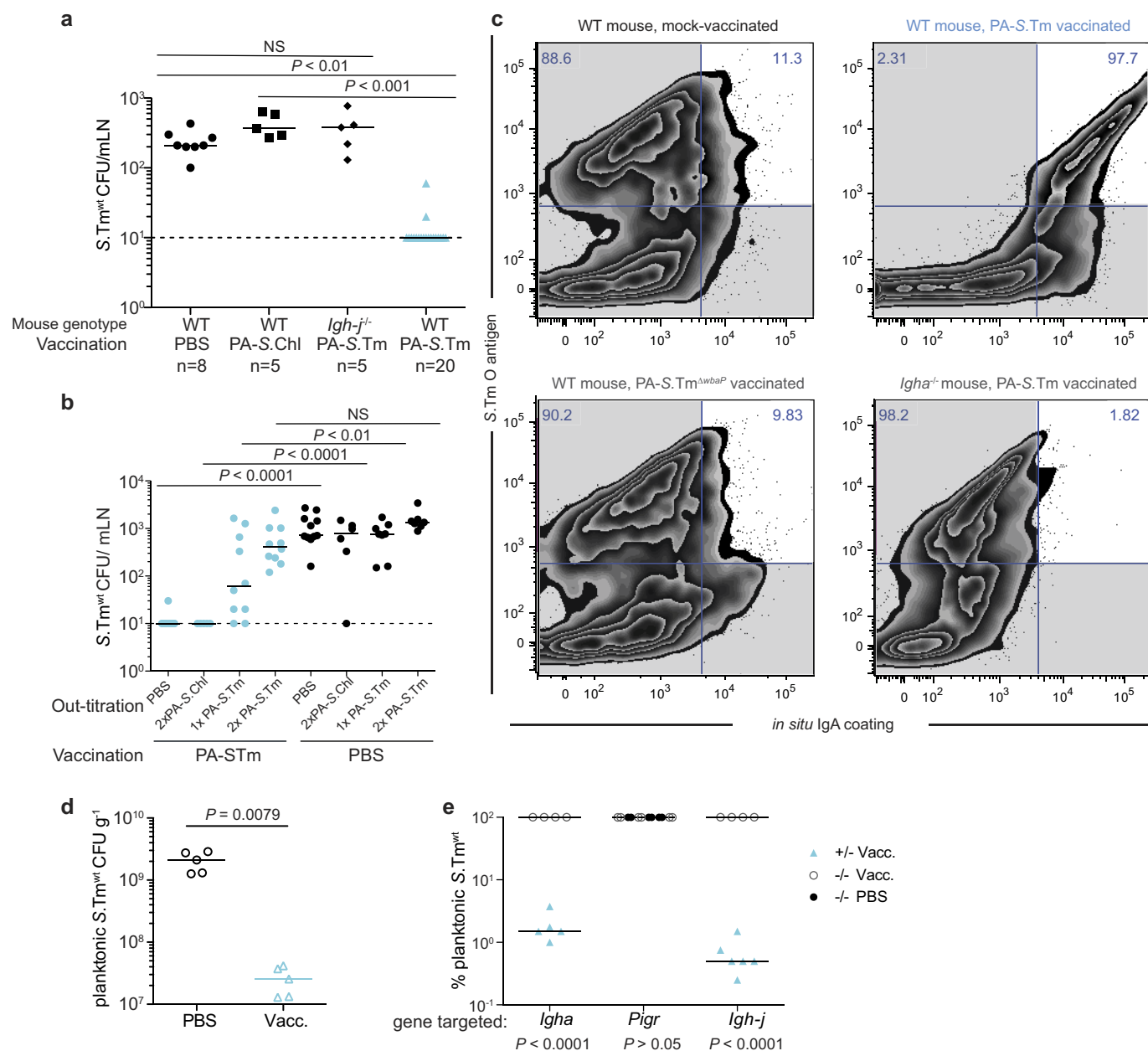
Mathematical modelling of the planktonic population kinetics in the presence of high-avidity IgA. See extended discussion in the Supplementary Information.
Code availability. Code used for data analysis and modelling was previously published[22,26], or is available from the corresponding authors on reasonable request.
Data availability. Numerical source data for all figures are provided with the paper. Imaging and flow cytometry raw data are available from the corresponding authors on reasonable request.

31. Müller, A. J. *et al. Salmonella* gut invasion involves TTSS-2-dependent epithelial traversal, basolateral exit, and uptake by epithelium-sampling lamina propria phagocytes. *Cell Host Microbe* **11,** 19–32 (2012).
32. Harriman, G. R. *et al.* Targeted deletion of the IgA constant region in mice leads to IgA deficiency with alterations in expression of other Ig isotypes. *J. Immunol.* **162,** 2521–2529 (1999).
33. Uren, T. K. *et al.* Role of the polymeric Ig receptor in mucosal B cell homeostasis. *J. Immunol.* **170,** 2531–2539 (2003).
34. Slack, E. *et al.* Innate and adaptive immunity cooperate flexibly to maintain host–microbiota mutualism. *Science* **325,** 617–620 (2009).
35. Diard, M. *et al.* Antibiotic treatment selects for cooperative virulence of *Salmonella typhimurium. Curr. Biol.* **24,** 2000–2005 (2014).
36. Hoiseth, S. K. & Stocker, B. A. Aromatic-dependent *Salmonella typhimurium* are non-virulent and effective as live vaccines. *Nature* **291,** 238–239 (1981).
37. Maier, L. *et al.* Microbiota-derived hydrogen fuels *Salmonella typhimurium* invasion of the gut ecosystem. *Cell Host Microbe* **14,** 641–651 (2013).
38. Stecher, B. *et al.* Flagella and chemotaxis are required for efficient induction of *Salmonella enterica* serovar Typhimurium colitis in streptomycin-pretreated mice. *Infect. Immun.* **72,** 4138–4150 (2004).
39. Ilg, K. *et al.* O-antigen-negative *Salmonella enterica* serovar Typhimurium is attenuated in intestinal colonization but elicits colitis in streptomycin-treated mice. *Infect. Immun.* **77,** 2568–2575 (2009).
40. Diard, M. *et al.* Inflammation boosts bacteriophage transfer between *Salmonella* spp. *Science* **355,** 1211–1215 (2017).
41. Nutter, R. L., Bullas, L. R. & Schultz, R. L. Some properties of five new *Salmonella* bacteriophages. *J. Virol.* **5,** 754–764 (1970).
42. Mobley, H. L. *et al.* Pyelonephritogenic *Escherichia coli* and killing of cultured human renal proximal tubular epithelial cells: role of hemolysin in some strains. *Infect. Immun.* **58,** 1281–1289 (1990).
43. Drecktrah, D. *et al.* Dynamic behavior of *Salmonella*-induced membrane tubules in epithelial cells. *Traffic* **9,** 2117–2129 (2008).
44. Gil, D. & Bouché, J. P. ColE1-type vectors with fully repressible replication. *Gene* **105,** 17–22 (1991).
45. Moor, K. *et al.* Analysis of bacterial-surface-specific antibodies in body fluids using bacterial flow cytometry. *Nat. Protocols* **11,** 1531–1553 (2016).
46. Traggiai, E. *et al.* An efficient method to make human monoclonal antibodies from memory B cells: potent neutralization of SARS coronavirus. *Nat. Med.* **10,** 871–875 (2004).
47. Helaine, S. *et al.* Dynamics of intracellular bacterial replication at the single cell level. *Proc. Natl Acad. Sci. USA* **107,** 3746–3751 (2010).
48. Sellin, M. E. *et al.* Epithelium-intrinsic NAIP/NLRC4 inflammasome drives infected enterocyte expulsion to restrict *Salmonella* replication in the intestinal mucosa. *Cell Host Microbe* **16,** 237–248 (2014).
49. Sommer, C., Strähle, C., Köthe, U. & Hamprecht, F. A. ilastik: Interactive Learning and Segmentation Toolkit. *Proc. Eighth IEEE International Symposium on Biomedical Imaging (ISBI).* **2011,** 230–233 (2011).
50. Kaiser, P. *et al.* Cecum lymph node dendritic cells harbor slow-growing bacteria phenotypically tolerant to antibiotic treatment. *PLoS Biol.* **12,** e1001793 (2014).
51. Berg, H. C. *Random Walks in Biology* (Princeton Univ. Press, 1993).
52. Jackson, G. A. A model of the formation of marine algal flocs by physical coagulation processes. *Deep-Sea Res. A, Oceanogr. Res. Pap.* **37,** 1197–1211 (1990).
53. Kiørboe, T., Andersen, K. P. & Dam, H. G. Coagulation efficiency and aggregate formation in marine phytoplankton. *Mar. Biol.* **107,** 235–245 (1990).
54. Lentle, R. G., Hemar, Y., Hall, C. E. & Stafford, K. J. Periodic fluid extrusion and models of digesta mixing in the intestine of a herbivore, the common brushtail possum (*Trichosurus vulpecula*). *J. Comp. Physiol. B* **175,** 337–347 (2005).
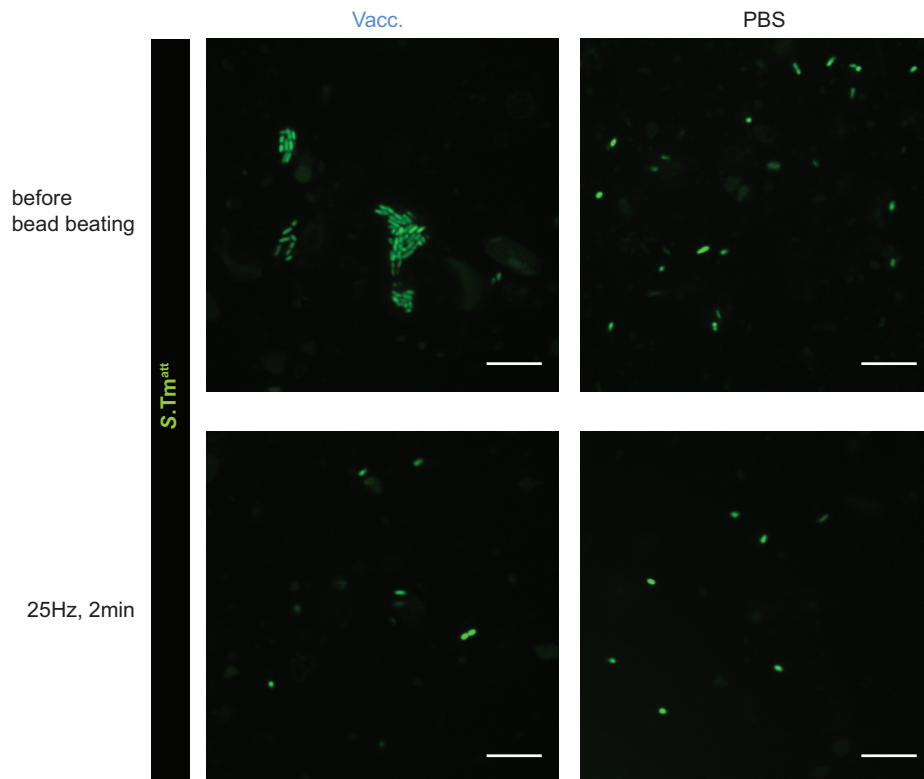
a — S.Tm^att CFU/g feces vs Time (h); inoculum size 10^3, 10^5, 10^7

b — % pAM34+ vs Time (h)

c — Log$_2$(% pAM34+) vs generations

y=-0.9(Log$_2$(% pAM34)) + 10.6

d — Generations vs Time (h)

Generations=2.05(Time)+0.29

e

generation:	1	2	3
% pAM34+:	100	50	25

Extended Data Figure 1 | *S.* Typhimurium growth in the streptomycin-treated mouse large intestine. Naive C57BL/6 SOPF mice ($n = 3$ per group, representative of 3 independent experiments) were gavaged with 25 mg streptomycin and 24 h later with the indicated inoculum of *S.*Tm^att carrying the conditionally replicating plasmid pAM34. **a**, CFU g^{-1} faeces with fitted four-parameter logistic (sigmoidal) curves by least-squares nonlinear regression. **b**, Percentage of the faecal population retaining ampicillin resistance at the indicated time points. Exponential decay curves were fitted by least-squares nonlinear regression. **c**, Calculation of a standard curve linking percentage plasmid carriage with generation number derived from serial dilution of the inoculum and overnight cultures *in vitro* (least squares linear regression of the log$_2$ percentage of plasmid carriage and calculated generation number, assuming zero death).

Note that the gradient is shallower than the expected value of 1. Low levels of residual IPTG-independent plasmid replication probably explain this. The *y* intercept is considerably greater than log$_2$(100) = 6.64, owing to the relatively high starting copy number (approximately $n = 16$) of the plasmid. **d**, Calculated numbers of generations in the caecum based on the data shown in **b** and **c**. Regardless of the starting inoculum, *S.* Typhimurium initially expands with a growth rate of approximately 2 h^{-1} until the caecal 'carrying capacity' is reached (linear regression of all values generated from a faecal *S.* Typhimurium density of <10^9 CFU g^{-1}). **e**, Illustration of plasmid loss (assuming perfect segregation; the analyses in **c** and **d** did not rely on this assumption) with a starting copy number of $n = 2$ (red circles, pAM34 plasmid).
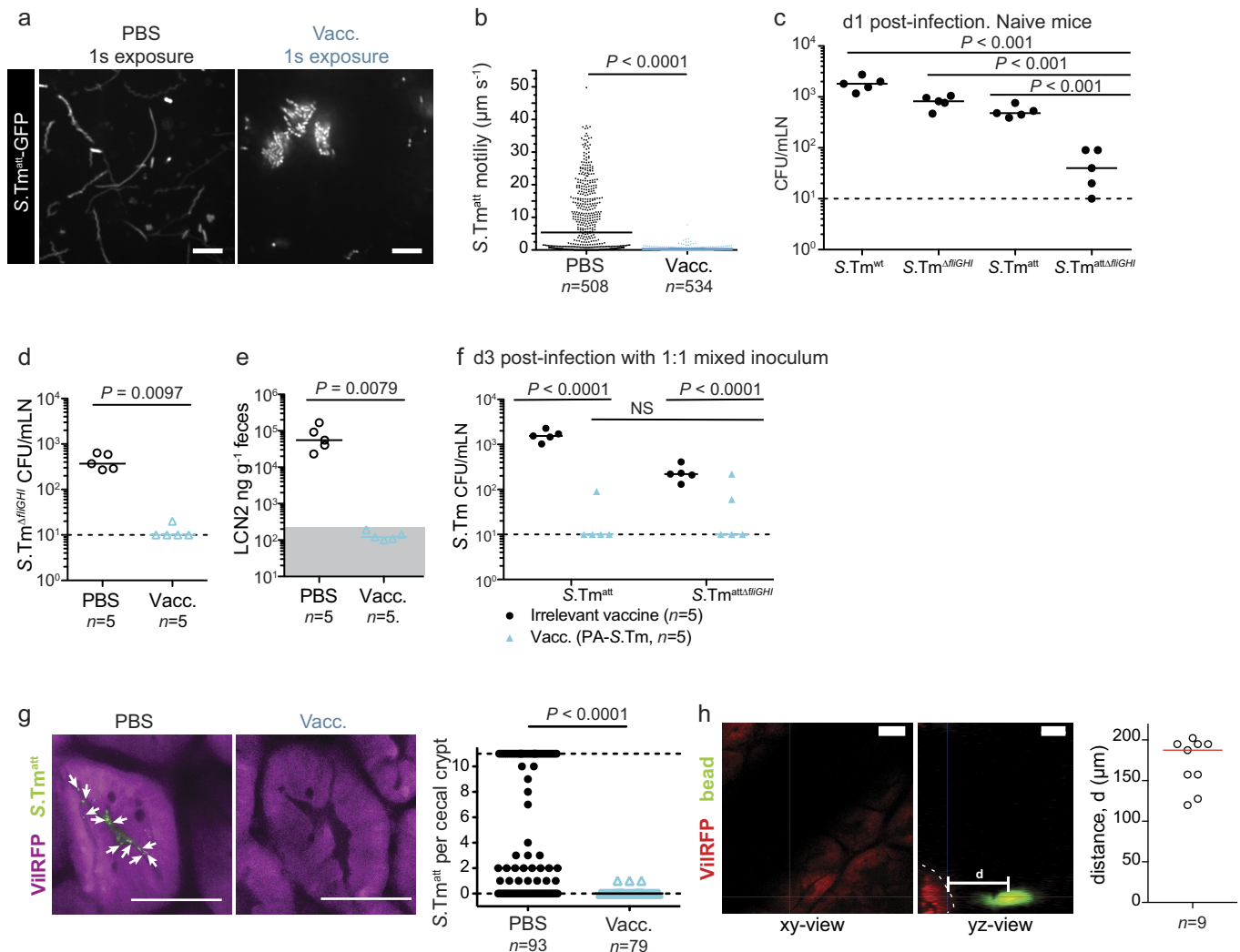
Extended Data Figure 2 | LPS-specific secretory IgA elicited by PA-S.Tm vaccination is necessary to prevent mLN translocation, coat S. Typhimurium in the caecum, and drive clumping. a, Wild-type and *Igh-j*^{−/−} C57BL/6 mice were vaccinated with mock vaccine (PBS), an inactivated *S*. Choleraesuis (O-antigen mismatched) vaccine (PAS.Chl) or PA-S.Tm, as indicated. On day 21 after the first vaccination, mice were pretreated with streptomycin and challenged with 10^5 S.Tm[WT]. mLN CFU were determined 18 h later. Kruskal–Wallis with Dunn's post hoc tests shown. **b**, C57BL/6 mice vaccinated with PA-S.Tm or PBS were streptomycin pretreated. 23.5 h later, animals were pretreated with 10^{11} particles of the indicated vaccine to specifically or non-specifically out-titrate IgA in the gut lumen. 30 min later, all animals were challenged with 10^5 S.Tm[WT] with (2×) or without (1×) a second 10^{11}-dose of the indicated vaccine preparation. mLN loads were determined at 24 h after infection. Dashed lines indicate detection limits. Two-way ANOVA on log-normalized data, with Bonferroni post hoc tests. **c**, Wild-type or *Igha*^{−/−} C57BL/6 mice were vaccinated as indicated and infected as in **a**. At 18 h after infection, caecal contents were stained with antibodies against IgA and against the *S*. Typhimurium O-antigen, and the staining intensities were analysed by flow cytometry. Representative zebra-plots (5% contours) showing *S*. Typhimurium O-antigen (human IgG anti-O12, Alexa647-anti-hIgG) and IgA staining (biotin anti-mouse IgA with Pacific-Blue–streptavidin) of caecal content bacteria. Non-shaded quadrant contains IgA-coated *S*. Typhimurium. Numbers denote the percentages of *S*. Typhimurium falling into each quadrant. **d**, **e**, Quantitative microscopy on intestinal content in fixed-frozen caecum sections from vaccinated wild-type (**d**), IgA-deficient (*Igha*^{−/−}), poly Ig receptor-deficient (*Pigr*) and fully antibody-deficient (*Igh-j*^{−/−}) C57BL/6 mice (**e**) vaccinated as indicated and infected as in (**a**). Kruskal–Wallis with Dunn's post hoc tests shown. Total luminal *S*. Typhimurium loads were not different between groups (data not shown). As vaccination with PA-S.Chl yielded identical results to mock-vaccination or fully antibody-deficient vaccinated mice, PBS-vaccinated controls were subsequently used unless otherwise stated.
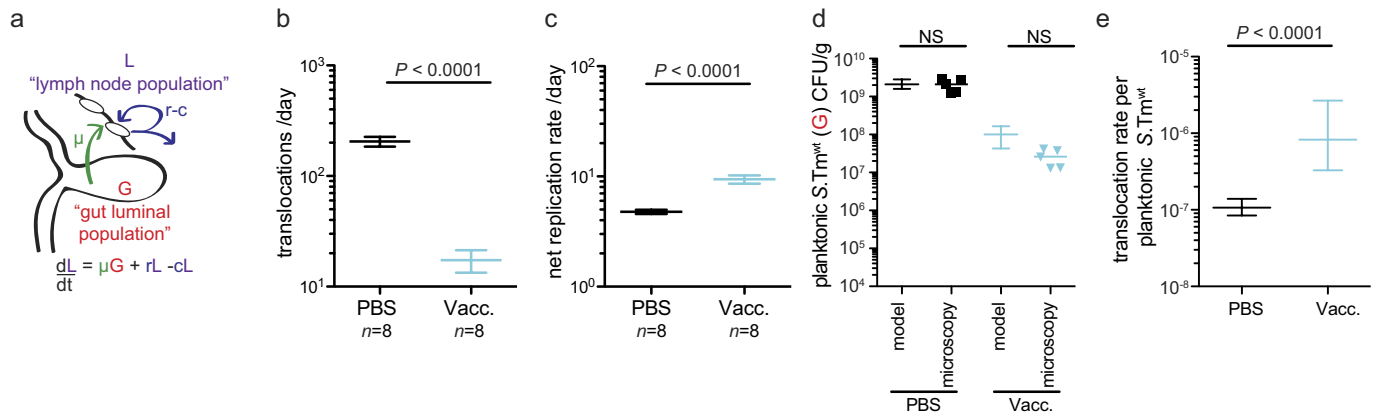
Extended Data Figure 3 | Owing to bead-beating, CFU can be determined correctly, even when secretory IgA clumps *S.* Typhimurium in the gut lumen. (See Fig. 1h for example.) Mock- (PBS) or PA-*S*.Tm- (vacc.) vaccinated mice were streptomycin pretreated and challenged with 10^5 CFU of *S*.Tm^{att} (pM965) constitutively expressing GFP. Caecal content was collected 24 h later and imaged directly after diluting 1 in 10 in PBS, or after bead-beating for 2 min at 25 Hz with a large sterile steel bead. Scale bar, 10 μm; representative images shown. Identical observations were made with *S*.Tm^{WT} (data not shown). Note, this verified that bead-beating (part of our routine analysis of caecum lumen, faecal and organ CFU analysis) efficiently breaks IgA-mediated clumps. Thus, plating is suitable for total CFU analysis in intestinal content of both naive and vaccinated mice.
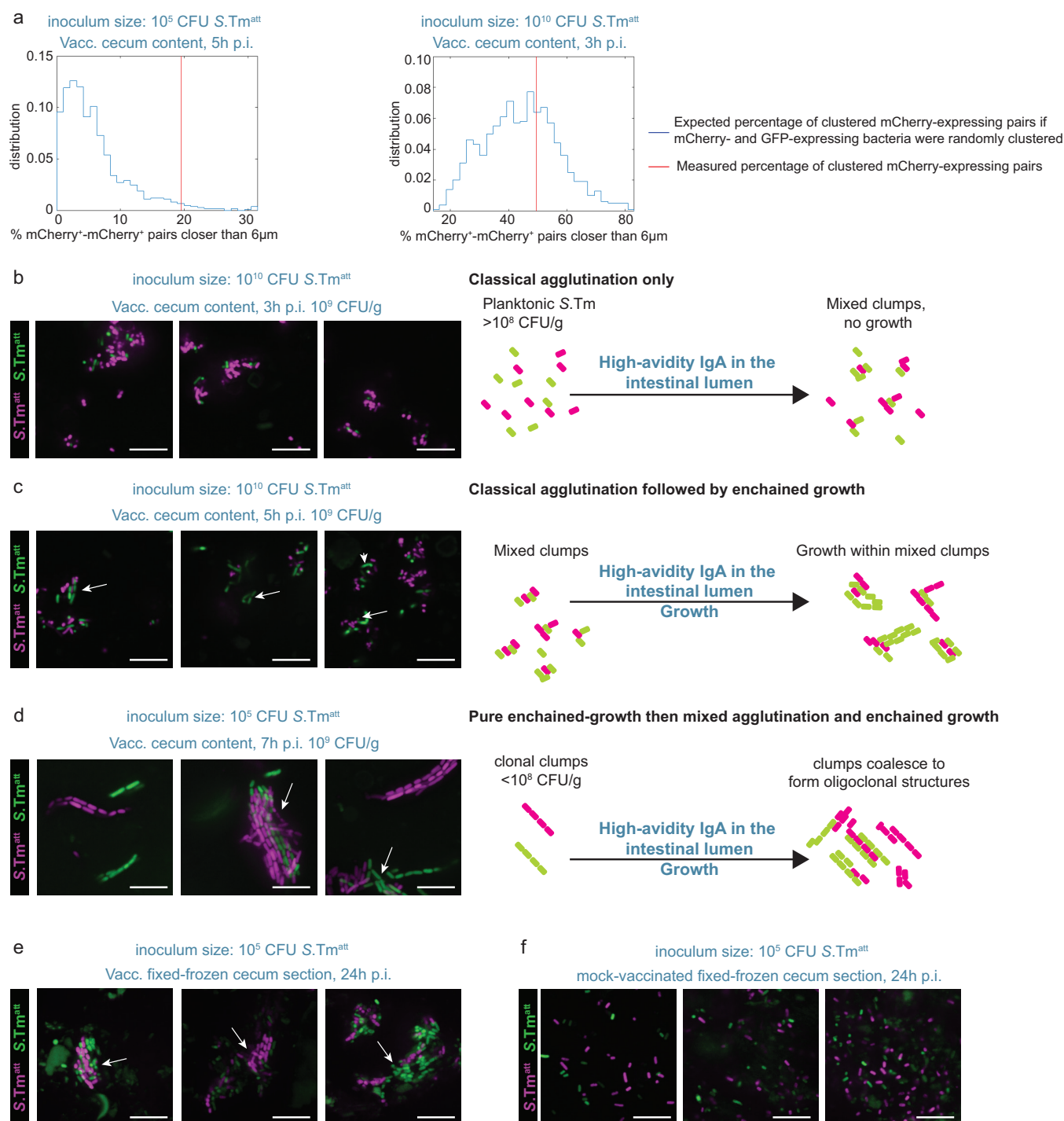
Extended Data Figure 4 | High-avidity IgA protects independently of blocking flagella-driven motility and type III secretion systems 1 and 2. a, Representative 1-s exposure confocal microscopy images of GFP-expressing S.Tm^{att} in live explanted caecal content 18 h after infection with 10^5 CFU. Tracks in the mock-vaccinated case indicate bacterial swimming during acquisition of the image. **b**, Microscopy quantification of S.Tm^{att} swimming speed. **c**, Naive mice ($n = 5$ per group) were pretreated with streptomycin and infected with 10^5 CFU of the indicated S. Typhimurium strain. mLN CFU at 24 h after infection; dashed line, lower detection limit. Kruskal–Wallis with Dunn's post hoc tests. **d**, **e**, Mock- (PBS) or PA-S.Tm-(vacc.) vaccinated mice were challenged with 10^5 CFU S.Tm$^{\Delta fliGHI}$ strain by gavage. We analysed mLN CFU at 18 h after infection (**d**); faecal lipocalin-2 at 18 h after infection (**e**). Two-tailed Mann–Whitney U-tests. **f**, Competitive infection experiments assessing the role of flagella in a S.Tm^{att} strain background. mLN CFU at day 3 after challenging vaccinated or mock-vaccinated mice ($n = 5$ per group) with a 1:1 mixture of 10^5 CFU S.Tm$^{att\Delta fliGHI}$ and S.Tm^{att}. Two-way ANOVA with Bonferroni post hoc tests. **g**, Mock- or PA-S.Tm-vaccinated $VilRPF$ mice were streptomycin pretreated and orally infected with 10^5 CFU of S.Tm^{att} (pM965) expressing

GFP constitutively. At 18 h after infection, mice were anaesthetized and artificially respirated. Caecal crypts were imaged by two-photon intravital confocal microscopy[31] (scale bar, 50 μm) and we quantified the number of S. Typhimurium per crypt. Very high numbers of S. Typhimurium were designated a maximum detection-limit of 11. n = number of crypts analysed per condition. Two-tailed Mann–Whitney U-tests. Clumps were located too deeply in the caecal content to be visualized by intravital microscopy across the caecal wall. **h**, $VilRPF$ mice were pretreated with streptomycin and, 24 h later, prepared for intravital confocal microscopy by injection of around 25-μm YG-fluorescent latex beads (green) directly into the caecal lumen, as an ultrabright proxy for bacterial aggregates. These beads were selected as having a similar diameter to an average S. Typhimurium clump in the gut lumen of vaccinated mice. Representative images depicting the bead location relative to the surface of the intestinal epithelium (white dashed line), and quantification (right). Scale bar, 50 μm. Note, the data shown in **g** and **h** suggest that secretory IgA-driven S. Typhimurium clusters are confined ≥ 100 μm away from the gut epithelium in PA-S.Tm-vaccinated mice, as cluster-sized beads are typically observed with at least this separation from the caecal epithelium.

Extended Data Figure 5 | Clumping-mediated depletion of planktonic, infectious $S.Tm^{WT}$ cells could fully account for the reduced mLN colonization in PA-$S.$Tm-vaccinated mice. We fitted a stochastic birth–death model modified by immigration, describing mLN colonization[22,50] in vaccinated mice to infection data with mixtures of barcoded $S.Tm^{WT}$ strains[25]. **a,** Scheme and statement of the deterministic model[22,50]. μ, translocation rate from the gut lumen to the mLN per $S.$ Typhimurium in the gut lumen (population size, G); $r - c$ (replication minus clearance = net replication rate of each $S.$ Typhimurium in the mLN (population size, L)). **b–e,** Mock- (PBS/irrelevant vaccine) or PA-$S.$Tm-vaccinated mice were pretreated with streptomycin and challenged with 10^5 CFU of $S.Tm^{WT}$, which was spiked with seven genetically barcoded strains ($S.Tm^{WT}$ background) at 1:35 of the total population. At 18 h after infection, mLN CFU determination and analysis of barcode abundance using qPCR were used to fit the mathematical model[22,50]. **b,** The translocation rate (μG) from the gut lumen to the mLN (Student's t-test, $P < 0.0001$). **c,** The net replication rate ($r - c$) in the mLN (Student's t-test, $P < 0.0001$). **d,** A comparison of the size of the luminal planktonic population (G) either empirically determined by microscopy counting and plating (symbols, as Extended Data Fig 2d) or predicted by dividing the predicted value of μG by the predicted value μ_{naive} (bootstrapped over 1,000 iterations to generate a median and 95%

confidence interval of the mean; see 'Modelling of translocation to the mLN' section in Methods). There is no significant difference between the predicted and measured values by two-way ANOVA. **e,** Translocation rate per planktonic $S.$ Typhimurium (μ) determined by dividing μG values determined by model-fitting by G values determined by microscopy (bootstrapping over 10^6 randomly sampled values from both normal distributions, used to generate mean (horizontal lines) and 95% confidence interval of the mean; Mann–Whitney U-test, $P < 0.0001$). Note, this data demonstrates that (1) if we assume that the translocation rate per infectious luminal $S.$ Typhimurium is unchanged in vaccination, our model predicts an identical decrease in the size of the luminal infectious population (that is, the planktonic $S.$ Typhimurium) as that which we can quantify by microscopy. In other words, the extent of clumping is sufficient to predict the observed decrease in mLN colonization when all other aspects of the infection are identical to naive animals. (2) Direct calculation of the translocation rate per infectious bacterium in vaccinated mice even suggests a slight increase in the predicted value of μ, consistent with a role for IgA in active sampling of luminal contents[1], but inconsistent with a loss of the function of type III secretion systems 1 and 2 *in vivo*[20]. Again, this shows that secretory IgA protects by clumping $S.$ Typhimurium deep in the gut lumen.
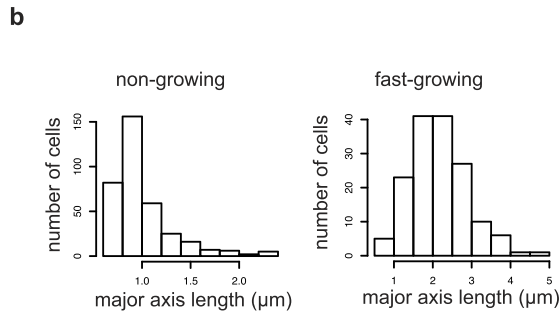
3

1

333

Extended Data Figure 6 | Enchained growth and classical agglutination can complement each other at high bacterial densities. a, Two representative plots quantifying the randomness of mCherry+ and GFP+ S. Typhimurium distribution in clusters. Blue histogram: predicted percentage of clustered mCherry+ pairs achieved when each bacterium in the images is randomly re-assigned mCherry or GFP expression (that is, simulated random agglutination) and the actual fraction determined by image analysis (red vertical line). The probability of observing this number of mCherry+ pairs in clusters if only random agglutination contributed was analysed for three mice that received a 10^5 CFU inoculum at 5 h after infection ($P = 0.006, 0.029, 0.048$); and three mice that received a 10^{10} CFU inoculum at 3 h after infection ($P = 0.36, 0.64, 0.24$). The distribution of fluorescence in clumps (Fig. 1i, j) is therefore significantly non-random after infection with realistic inocula, but not high inocula. **b–d**, PA-S.Tm-vaccinated C57BL/6 mice were pretreated with ampicillin and infected with the indicated inoculum of S.Tm^{att} constitutively expressing green (GFP; pM965) or red (mCherry; pFPV25.1) fluorescent proteins. **b–d**, Mice were killed at the indicated times after infection and caecal content explants directly imaged by confocal microscopy. Representative images and schematic diagrams depicting the corresponding processes. **e, f**, Mice infected as indicated were killed at 24 h after infection. Fixed, frozen 25-μm caecum sections were imaged by confocal microscopy.

© 2017 Macmillan Publishers Limited, part of Springer Nature. All rights reserved.

a Change in planktonic population size = Change due to agglutination + Change due to enchained growth

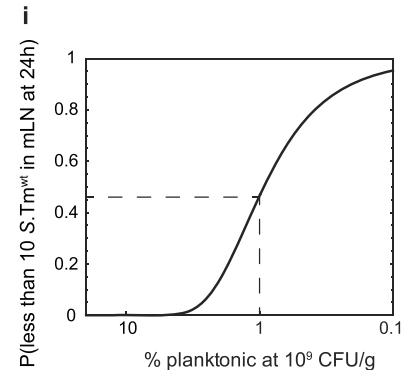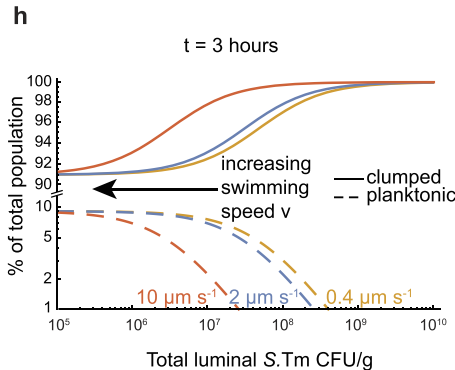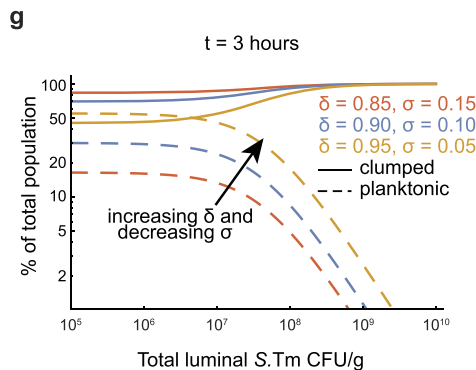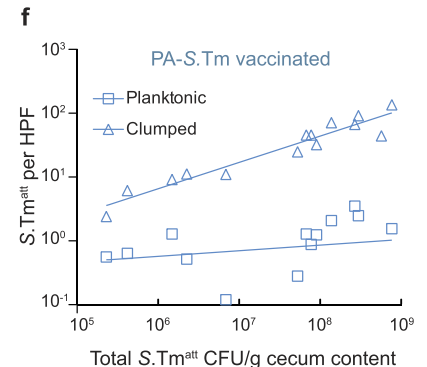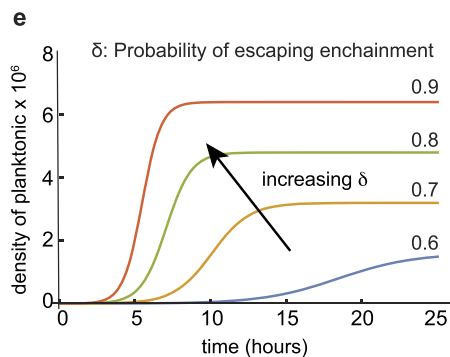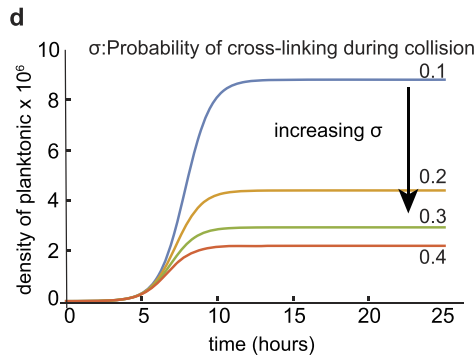$$\frac{dC}{dt} = \frac{dC}{dt}\bigg|_{CA} + \frac{dC}{dt}\bigg|_{EG} = \frac{dC}{dt}\bigg|_{mot} + \frac{dC}{dt}\bigg|_{mix} + \frac{dC}{dt}\bigg|_{grow}$$

$$\frac{dC}{dt} = -16\pi a\sigma D C^2 - 10.4\sigma a^3 \left(\frac{\epsilon}{\nu}\right)^{0.5} C^2 + (2\delta - 1)\lambda C$$

b

non-growing

fast-growing

c

Parameter	Symbol	Value (Source)
Cell radius	a	growing: 2.15μm, non-growing: 1.0μm
Average run time	τ	0-1s (Berg, H. C. *Random walks in biology.* (Princeton University Press, 1993))
Kinematic viscosity of fluid	ν	8×10^{-4} m²/s $=2.9\times10^{12}$ μm²/h (*Journal of Comparative Physiology B* **175**, 337-347 (2005))
Cell growth rate	λ	2 h⁻¹ (Extended Data Fig. 1d)
Probability of cross-linking during collision	σ	Possible values: $0 \leq \sigma \leq 1$ (Robust fit to experimental data - Fig. 1k)
Probability of escaping enchainment	δ	Possible values: $0.5 \leq \delta \leq 1$ (Robust fit to experimental data - Fig. 1k)
Cell swimming speed	v	Possible values: 0 μm/s $\leq v \leq$ 10 μm/s (Fig. 4b)
Turbulent mixing dissipation rate	ϵ	10^{-2} W/kg (Conservative upper bound. *Journal of Comparative Physiology B* **175**, 337-347 (2005))
Cosine of angle between runs	α	0.33 (Berg, H. C. *Random walks in biology.* (Princeton University Press, 1993))
Diffusivity	$D = \frac{v^2\tau}{3(1-\alpha)}$	(Derived from above terms)

d

e
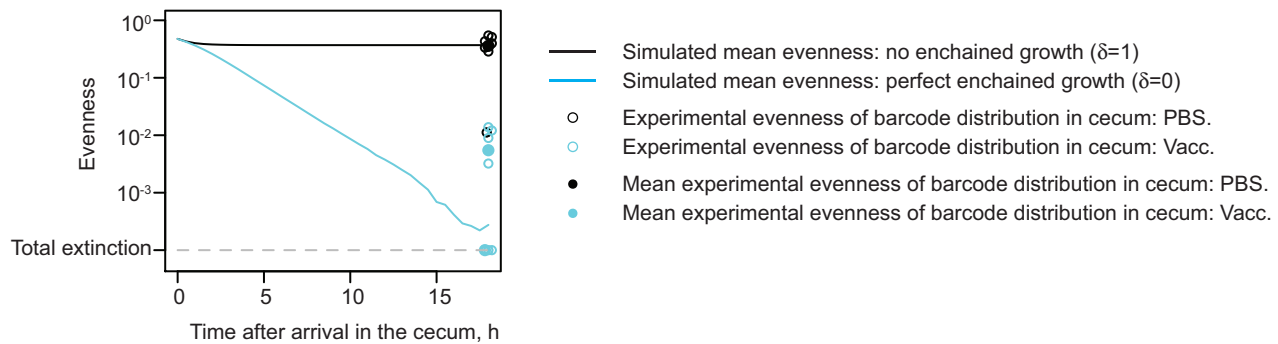

f

g

h

i

Extended Data Figure 7 | See next page for caption.

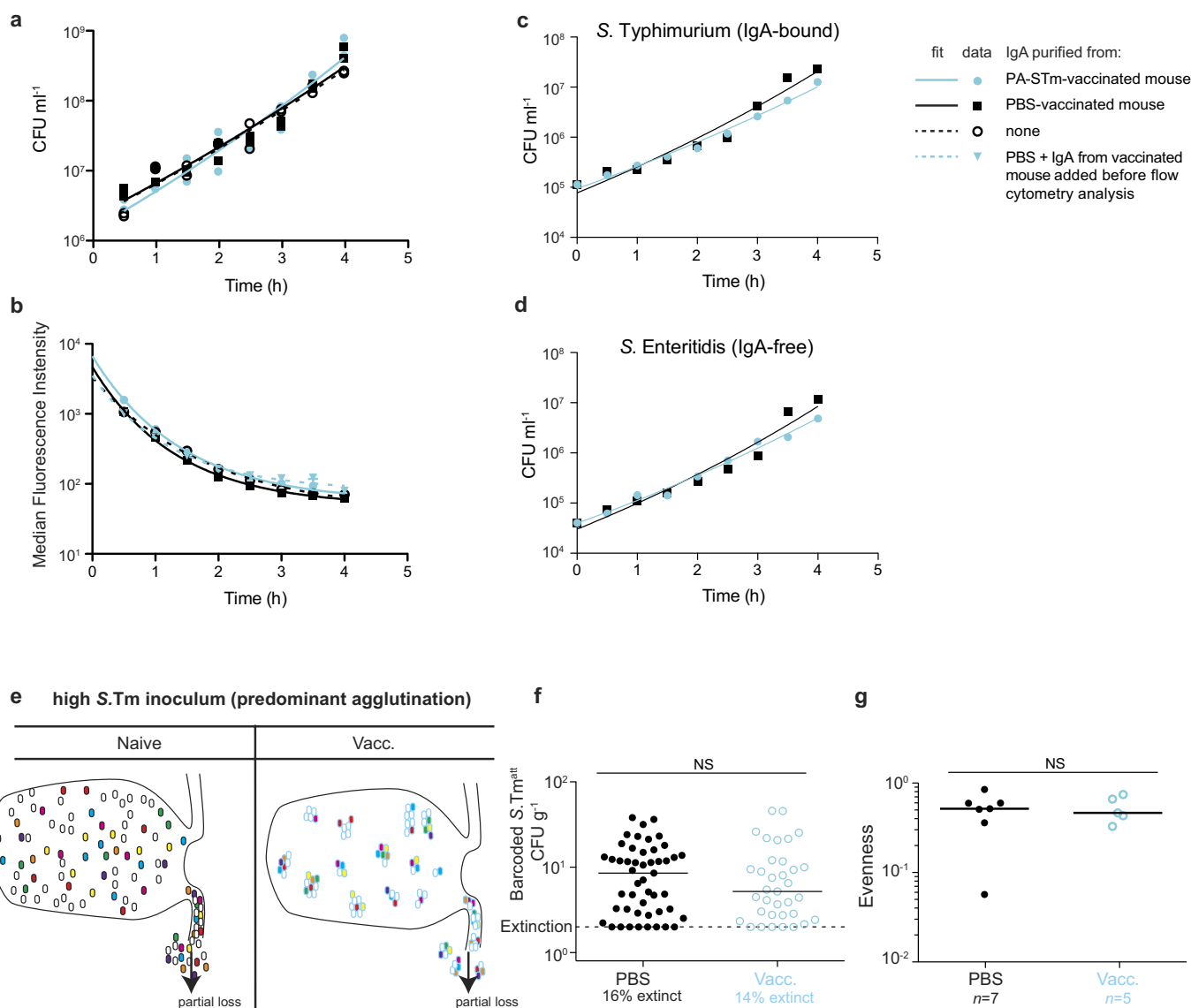**Extended Data Figure 7 | Modelling the effect of enchained growth and classical agglutination on clumping and the density of planktonic *S.* Typhimurium in the caecal lumen. a**, Equations governing the model, where *C* is the concentration of planktonic bacteria, *t* is time in hours and the subscripts CA and EG indicated 'classical agglutination' and 'enchained growth', respectively. **b**, Determination of cell radius from confocal fluorescence microscopy images of live explanted caecal content at 3 h post-infection with 10^{10} CFU (non-growing) or 5 h after infection with 10^5 CFU (fast-growing) *S.*Tm^att. **c**, All parameters used in the model including references to their origin[51–54]. **d**, **e**, Predicted density of planktonic bacteria over 24 h of exponential growth in the caecal lumen. Note that at late time points (high density of CFU), the planktonic population reaches a true equilibrium. **d**, Altering σ (efficiency of classical agglutination) for a fixed value of δ. Note that altering the efficiency of classical agglutination alters the size of the equilibrium planktonic population, but not the rate of increase. **e**, Decreasing the efficiency of enchained growth (that is, increasing δ) increases both the size of the planktonic population and the rate at which the population increases during exponential growth. **f**, Quantification of *S.* Typhimurium planktonic and clumped bacteria per high-power field in microscopy of explanted live caecal content from PA-*S.*Tm-vaccinated mice challenged with *S.*Tm^att (10^5 CFU). This supports the model of an equilibrium planktonic population size that remains constant, as the clumped population exponentially expands. **g**, The predicted percentage of the population that is clumped (solid lines) and planktonic (dashed lines) when the efficiency of enchained growth decreases (that is, increasing δ) at 3 h after infection. **h**, As in **g**, but flagella-driven swimming speed is re-introduced for fixed values of $\delta = 0.8$ and $\sigma = 0.2$. Note that increasing swimming speed increases the efficiency of classical agglutination, potentially improving protection. **i**, Linking enchained growth to vaccine-mediated protection. On the basis of the stochastic model presented in Extended Data Fig. 5a, we can calculate the probability of recovering 10 CFU of *S.* Typhimurium from the mLN at day 1 after infection as a function of the percentage of luminal bacteria that are planktonic. The dashed lines indicate that in the case of a 100-fold reduction in the planktonic population, we expect less than 10 CFU *S.* Typhimurium in the mLNs in approximately 50% of the animals.
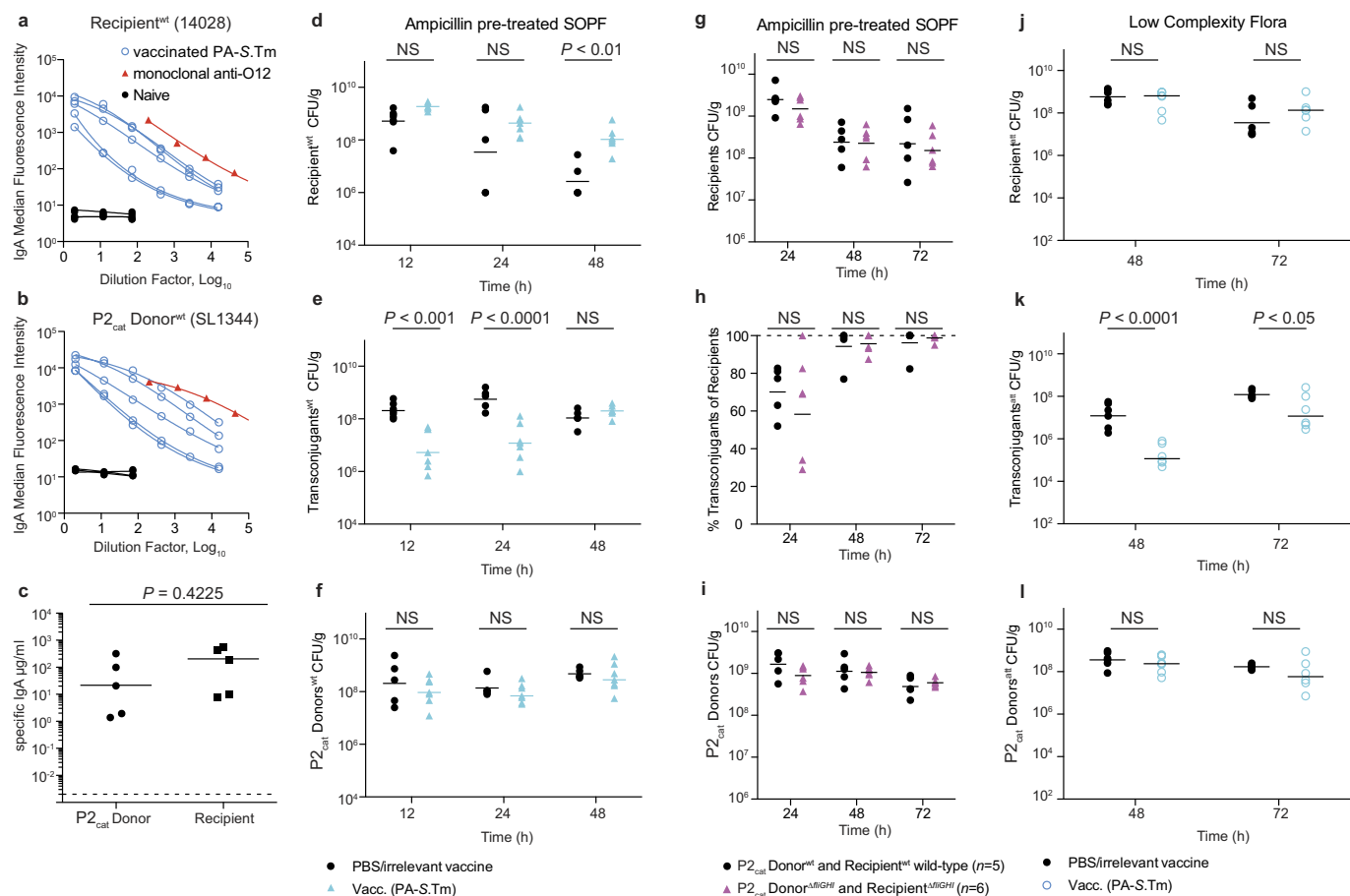
Extended Data Figure 8 | Simulating the effect of IgA-driven enchained growth on clonal extinction in the caecal lumen. In order to visualize how enchained growth leads to clonal extinction without killing, we simulated a simple scenario on the basis of the experiments of Fig. 2b, c (see Supplementary Methods). Approximately 10 CFU of each of seven barcoded clones arrive in the caecum. These bacteria get established in the caecum with probability $P = 0.115$ (based on the loss of evenness in unvaccinated animals). The remaining bacteria double every 30 min during the first 12 h. Growth then slows for the next 6 h as the carrying capacity is reached (typical of infection kinetics with 10^5 CFU *S.* Typhimurium in a streptomycin-pretreated mouse). 10% of the caecal content is cleared to the colon every 15 min to produce faeces. We simulated the extreme cases of no enchained growth ($\delta = 1$, black line), or a 'perfect' enchained growth ($\delta = 0$, cyan line). The 'evenness'[26], that is, the similarity of the proportions of each barcode in the population, of 300,000 simulations of this simplified model up to 18 h after infection was computed and averaged. In the naive case (that is, no enchained growth, $\delta = 1$, black line), the evenness stabilizes after 1 h, at a value of the same order of magnitude than the median experimental value for the unvaccinated mice. In the case of perfect enchained growth ($\delta = 0$, cyan line), the evenness continues to drop, indicating on-going clonal extinction. The experimental evenness achieved in vaccinated animals at 18 h after infection (cyan open circles represent individual mice, mean evenness of all six animals is represented as a cyan filled circle, as in Fig. 2c) is located between the simulated final values of evenness with no enchained growth and with perfect enchained growth, qualitatively consistent with the idea that enchained growth *in vivo* is not 100% efficient (for example, due to breaking or collision of clonal clumps, Extended Data Fig. 7).

a, **b**,

fit   data   IgA purified from:
— PA-STm-vaccinated mouse
— PBS-vaccinated mouse
--- none
--- PBS + IgA from vaccinated mouse added before flow cytometry analysis

c *S.* Typhimurium (IgA-bound)

d *S.* Enteritidis (IgA-free)

e high *S.*Tm inoculum (predominant agglutination)

f NS PBS 16% extinct Vacc. 14% extinct

g NS PBS n=7 Vacc. n=5

Extended Data Figure 9 | Direct toxicity cannot explain clonal extinction. a, b, An overnight culture of *S.*Tm^att carrying an arabinose-inducible GFP (pBADGFPmut2) was diluted 1 in 100 into LB (1% w/v arabinose) with ampicillin selection for 3 h to fully induce the reporter. Subsequently, the bacteria were thoroughly washed and diluted 1:100 into fresh LB that was free of arabinose and contained secretory IgA purified from the small-intestinal lavages of mock- (PBS) or PA-*S.*Tm- (vacc.) vaccinated mice, similarly to previously described fluorescence-dilution assays[47]. Samples were removed and clusters disrupted by bead-beating (Extended Data Fig. 3) for plating and flow cytometry every 30 min for 4 h (n = 2 independent experiments, pooled). **a,** CFU ml^−1, as determined by plating. **b,** Median GFP fluorescence intensity, as determined by flow cytometry. An additional control for the effect of agglutination on fluorescence intensity was carried out by adding purified IgA from PA-*S.*Tm vaccinated mice to an IgA-free sample just before flow cytometry staining. P > 0.05 by repeat-measures ANOVA on log-normalized data. This indicates no detectable effect of specific IgA on *S.* Typhimurium growth or viability *in vitro*. **c, d,** *S.*Tm^att WITS carrying a neutral kanamycin-resistance cassette and *S.* Enteritidis carrying a growth-neutral chloramphenicol-resistance cassette (M1513) were cultured separately overnight in LB. These cultures were mixed 1:1, then diluted 1:100 into LB

without antibiotics, and supplemented with IgA purified from PA-*S.*Tm-vaccinated (cyan) or PBS-treated mice (black) as above. Every 30 min a sample was removed and clusters disrupted by bead-beating (Extended Data Fig. 3). CFU ml^−1 of the IgA-bound strain (*S.* Typhimurium) (**c**) and IgA-non-bound strain (*S.* Enteritidis) (**d**) were determined by selective plating. P > 0.05 by repeat-measures ANOVA on log-normalized data. One representative experiment of two. The expected patterns of IgA-coating were confirmed at the end of each experiment by bacterial flow cytometry. IgA-mediated effects do not selectively disadvantage *S.* Typhimurium growth in the presence of rich media. **e–g,** Classical agglutination does not drive clonal extinction. Mock- or PA-*S.*Tm-vaccinated mice were orally infected with an inoculum of 10^10 CFU of *S.*Tm^att, spiked with approximately 10 CFU of each of seven genetically barcoded kanamycin-resistant *S.*Tm^att strains. **e,** Scheme depicting the expected effect of agglutination on clonal loss. Fill colours, barcodes; blue outlines, secretory-IgA-coated bacteria. **f,** The number of CFU of each barcoded strain was determined in the caecal lumen at 18 h after infection by selective plating, enrichment culture and qPCR[22,50]. **g,** Evenness[26] of the resulting barcoded population in each animal analysed. Mann–Whitney U-test statistics are shown.

Extended Data Figure 10 | Raw data for conjugative plasmid transfer in vaccinated mice. (See Figs 3 and 4.) **a–c**, Small-intestinal lavages from PA-*S*.Tm-vaccinated or naive mice were titrated against wild-type recipient (14028 *S*. Typhimurium) (**a**) and P2$_{cat}$ wild-type donor (SL1344 *S*. Typhimurium) (**b**) and compared to a monoclonal dimeric mouse IgA directed against the O12 antigen. **a**, **b**, Raw titration curves. **c**, Absolute titres defined relative to an O12-specific monoclonal dimeric IgA. Two-tailed Mann–Whitney *U*-test, not significant. **d–f**, C57BL/6 SOPF mice were orally vaccinated with PA-*S*.Tm (vacc.), PA-inactivated *S*. Choleraesuis or PBS only (irrelevant vaccine/PBS). On day 21 after the first vaccination, all mice were pretreated with ampicillin and mice were sequentially infected with 10^2 CFU each of P2$_{cat}$ wild-type donor and wild-type recipient *S*. Typhimurium. **d**, Loads of kanamycin-resistant wild-type recipient in the faeces. **e**, Loads of kanamycin–chloramphenicol-double-resistant transconjugants in the faeces. **f**, Loads of chloramphenicol-resistant P2$_{cat}$ wild-type donor, determined from faecal samples by selective plating (corresponding to data in Fig. 3a). **g–i**, Naive C57BL/6

SOPF were pretreated with ampicillin. 24 h later, mice were sequentially infected with either 10^2 CFU each of P2$_{cat}$ wild-type donor or P2$_{cat}$ $\Delta fliGHI$ donor and wild-type recipient or $\Delta fliGHI$ recipient, respectively. **g**, Loads of kanamycin-resistant plasmid-negative recipient in the faeces. **h**, Percentage of transconjugants, of the total recipient population in faeces. **i**, Loads of chloramphenicol-resistant P2$_{cat}$ donors. *S*.Tm^{WT} versus *S*.Tm$^{\Delta fliGHI}$ $P > 0.05$ by repeat-measures two-way ANOVA on log-normalized data. **j–l**, Mice with low-complexity microflora were orally vaccinated as in **d**. On day 21 after the first vaccination, all mice were infected sequentially with 200 CFU each of P2$_{cat}$ attenuated donor and attenuated recipient without antibiotic pretreatment. **j**, Loads of kanamycin-resistant attenuated recipient in the faeces. **k**, Loads of kanamycin–chloramphenicol-double-resistant transconjugants in the faeces. **l**, Loads of chloramphenicol-resistant P2$_{cat}$ attenuated donor, determined from faecal samples by selective plating (corresponding to data in Fig. 4a). **d–l**, Repeat-measures ANOVA on log-normalized data. Bonferroni post hoc tests shown.